Leadership Through Influence: What Mechanisms Allow Leaders to Steer a Swarm?

(Article begins on next page)

24 September 2024

Society for
Mathematical
Biology

Check for
updates

ORIGINAL ARTICLE

Leadership Through Influence: What Mechanisms Allow Leaders to Steer a Swarm?

Sara Bernardi[1] · Raluca Eftimie[2] · Kevin J. Painter[3]

Abstract

Collective migration of cells and animals often relies on a specialised set of "leaders", whose role is to steer a population of naive followers towards some target. We formulate a continuous model to understand the dynamics and structure of such groups, splitting a population into separate follower and leader types with distinct orientation responses. We incorporate *leader influence* via three principal mechanisms: a bias in the orientation of leaders towards the destination (orientation-bias), a faster movement of leaders when moving towards the target (speed-bias), and leaders making themselves more clear to followers when moving towards the target (conspicuousness-bias). Analysis and numerical computation are used to assess the extent to which the swarm is successfully shepherded towards the target. We find that successful leadership can occur for each of these three mechanisms across a broad region of parameter space, with conspicuousness-bias emerging as the most robust. However, outside this parameter space we also find various forms of unsuccessful leadership. Forms of excessive influence can result in either swarm-splitting, where the leaders break free and followers are left rudderless, or a loss of swarm cohesion that leads to its eventual dispersal. Forms of low influence, on the other hand, can even generate swarms that move away from the target direction. Leadership must therefore be carefully managed to steer the swarm correctly.

✉ Sara Bernardi
   sara.bernardi@polito.it

   Raluca Eftimie
   raluca.eftimie@univ-fcomte.fr

   Kevin J. Painter
   kevin.painter@polito.it

[1] Dipartimento di Scienze Matematiche (DISMA), Politecnico di Torino, Corso Duca degli Abruzzi 24, 10129 Turin, Italy

[2] Laboratoire de mathématiques de Besançon, UMR-CNRS 6623, Université de Bourgogne Franche-Comté, 16 Route de Gray, 25000 Besançon, France

[3] Dipartimento Interateneo di Scienze, Progetto e Politiche del Territorio (DIST), Politecnico di Torino, Viale Pier Andrea Mattioli, 39, 10125 Turin, Italy

🍃 Springer

1 Introduction

Collective migration underlies numerous processes, including the migration of cells during morphogenesis and cancer progression (Friedl and Gilmour 2009; Friedl et al. 2012), social phenomena such as pedestrian flow and crowding (Helbing and Molnar 1995; Kretz et al. 2006; Colombi et al. 2017), and the coordinated movements of animal swarms, flocks and schools (Dingle 2014; Westley et al. 2018).

In many cases, effective migration may demand the presence or emergence of *leaders*, for example, as an evolved strategy for herding the population to a certain destination, finding better environments, hunting or escaping, *etc*. At the cellular level, examples include epithelial wound healing, where a set of so-called leader cells at the tissue boundary appear to guide a migrating cell group (Vishwakarma et al. 2018), embryonic neural crest cell invasion, where trail-blazing pioneers lead followers in the rear (Schumacher et al. 2016), and kidney morphogenesis, where the lumen forms as leading cells leave the epithelialised tube in their wake (Atsuta and Takahashi 2015). Collective invasion of breast cancer appears to be driven by a specialised population defined by their expression of basal epithelial genes (Cheung et al. 2013).

Leadership is also found in various migrating animal groups, for example, arising from a cohort of braver or more knowledgeable individuals: faced by poor feeding grounds, post-reproductive females take on an apparent leadership role in the guidance of a killer whale pod, their experience offering a reserve of ecological knowledge (Brent et al. 2015). As our principal motivation, we consider honey bee swarms, which form as a colony outgrows its nest site. At this point, the queen and two-thirds of the colony depart (leaving a daughter to succeed her) and temporarily bivouac nearby, for example, on a tree branch. Over the following hours to days, a relatively small subpopulation of *scout bees* (∼3–5% of the 10,000+ strong swarm) scour the surroundings for a suitable new nest location, potentially several kilometres distant. The quality of a potential site is broadcast to other swarm members and, once consensus is obtained, the entire colony moves to the new dwelling. Consequently, guidance of thousands of naive insects (including the queen) is entrusted to a relatively small number of informed scouts (Seeley 2010). Observations suggest that scouts perform a sequence of high-velocity movements towards the nest site through the upper swarm (Beekman et al. 2006; Schultz et al. 2008; Greggers et al. 2013; Seeley 2010), "streaking" that conceivably increases their conspicuousness and communicates the nest direction.

Understanding the collective and coordinated dynamics of migrating groups demands analytical reasoning. The mathematical and computational literature in this field encompasses a particularly wide range of approaches. Microscopic, agent-based or individual-based models describe a group as a collection of individual agents, where the evolution of each particle is tracked over time. Benefiting from their capacity to provide a quite detailed description of an agent's dynamics, they offer a relatively natural tool to investigate collective phenomena (see, for instance, Couzin et al. 2005,

2002; Diwold et al. 2011; Fetecau and Guo 2012; Janson et al. 2005; Ioannou et al. 2015; Bernardi et al. 2018).

However, as the number of component individuals becomes large (as would be typical for many cancerous populations, large animal groups, *etc*), microscopic methods become computationally expensive and macroscopic approaches may become necessary. Various continuous models have been proposed to understand the collective migration dynamics of interacting populations, with *nonlocal PDE* frameworks becoming increasingly popular; models falling into this class have been developed in the context of both ecological and cellular movements, e.g. see Mogilner and Edelstein-Keshet (1999), Armstrong et al. (2006), Topaz et al. (2006), Eftimie et al. (2007), Eftimie (2012). Their nonlocal nature stems from accounting for the influence of neighbours on the movements of an individual, and their relative novelty has also become a source of significant mathematical interest (see Chen et al. 2020 for a review).

The aim of this paper is to investigate the impact of informed leaders on naive followers, using a nonlocal PDE model that builds on the hyperbolic PDE approach developed in Eftimie et al. (2007). In particular, we will explore the extent to which the presence of leaders can result in a *steered swarm*, defined as a population acquiring and maintaining a *spatial compact profile* that is *consistently steered* towards a target known only to the leaders. Motivated by real-world case studies (in particular, bee swarming as described above), we assume leaders attempt to influence the swarm using one or more of three mechanisms: (i) leaders preferentially choose the direction of the target; (ii) the leaders moving towards the target move more quickly than the leaders that are moving away from the target; (iii) leaders that are moving towards the target are more conspicuous than those moving away from the target, for example, through making themselves more visible to the followers. In Sect. 2, we introduce the full follower–leader model, along with two simple submodels—a leaders-only and a followers-with-implicit-leaders system—designed to reveal insights into the behaviour of the full system. Section 3 explores the dynamics of the submodels, via a combination of linear stability and numerical simulation. Section 4 subsequently addresses the full system, in particular the effectiveness of different biases. We conclude with a discussion and an outlook of future investigations.

2 Follower–Leader Swarm Model

We assume a heterogeneous swarm composed of distinct populations of knowledgeable leaders and naive followers. Both orient according to their interactions with other swarm members, as detailed below, but leaders have "knowledge" of the target and therefore the direction in which the swarm should be steered. For convenience, we will restrict here to one space dimension, assume fixed speeds, and account for direction through separately tracking positively $(+)$ and negatively $(-)$ oriented populations. Without loss of generality, we assume the leaders aim to herd the swarm in the $(+)$ direction, influencing via:

– *O-bias, orientation.* Leaders preferentially choose the target direction.

– *S-bias, speed.* Leaders moving towards the target move faster than leaders moving away from the target.
– *C-bias, conspicuousness.* Leaders moving towards the target are more conspicuous to followers than leaders moving away from the target, e.g. through specific behaviour.

Over the following pages, we present the model, introducing and describing the equations step by step. For compactness, we employ $\pm$ notation; however, for the reader's benefit we have expanded this notation within a complete listing of the equations in Appendix A. Setting $u^\pm(x, t)$ and $v^\pm(x, t)$ to denote the densities of followers and leaders, respectively, at position $x \in \Omega \subset \mathbb{R}$ and time $t \in [0, \infty)$, the governing equations are as follows:

$$
\begin{aligned}
\frac{\partial u^+}{\partial t} + \gamma \frac{\partial u^+}{\partial x} &= -\lambda^{u^+} u^+ + \lambda^{u^-} u^-, \\
\frac{\partial u^-}{\partial t} - \gamma \frac{\partial u^-}{\partial x} &= +\lambda^{u^+} u^+ - \lambda^{u^-} u^-, \\
\frac{\partial v^+}{\partial t} + \beta_+ \frac{\partial v^+}{\partial x} &= -\lambda^{v^+} v^+ + \lambda^{v^-} v^-, \\
\frac{\partial v^-}{\partial t} - \beta_- \frac{\partial v^-}{\partial x} &= +\lambda^{v^+} v^+ - \lambda^{v^-} v^-, \\
u^\pm(x, 0) &= u_0^\pm(x), \\
v^\pm(x, 0) &= v_0^\pm(x).
\end{aligned}
\tag{1}
$$

In its general setting, the model is formulated under the assumption of an infinite 1D line. For the simulations later, we consider a bounded interval $\Omega = [0, L]$, but wrapped onto the ring (periodic boundary conditions) to minimise the influence of boundaries. Initial conditions will be specified later.

In the above model, followers move with a fixed speed (set at γ). Leaders have potentially distinct speeds, $\beta_\pm$, according to whether **S-bias** is in operation; for example, in the case of bee swarming, scouts engage in streaking and increase their speed when moving towards the new nest site (Seeley 2010). Switching between directions is accounted for via the right hand side terms, where λ^{u^+} denotes the rate at which a follower (u) turns from $(+)$ to $(-)$, with similar definitions for λ^{u^-}, $\lambda^{v^\pm}$. Note that the current model excludes switching between follower and leader status, although it is of course possible to account for such behaviour through additional role-switching transfer functions.

The turning rate functions are based on interactions between swarm members where, accounting for the "first principles of swarming" (Carrillo et al. 2010), we combine *repulsion* (preventing collision between swarm members), *attraction* (preventing loss of contact and swarm dispersal), and *alignment* (choosing a direction according to those assumed by neighbours and/or external bias). Figure 1 summarises the general principals upon which the model is founded.
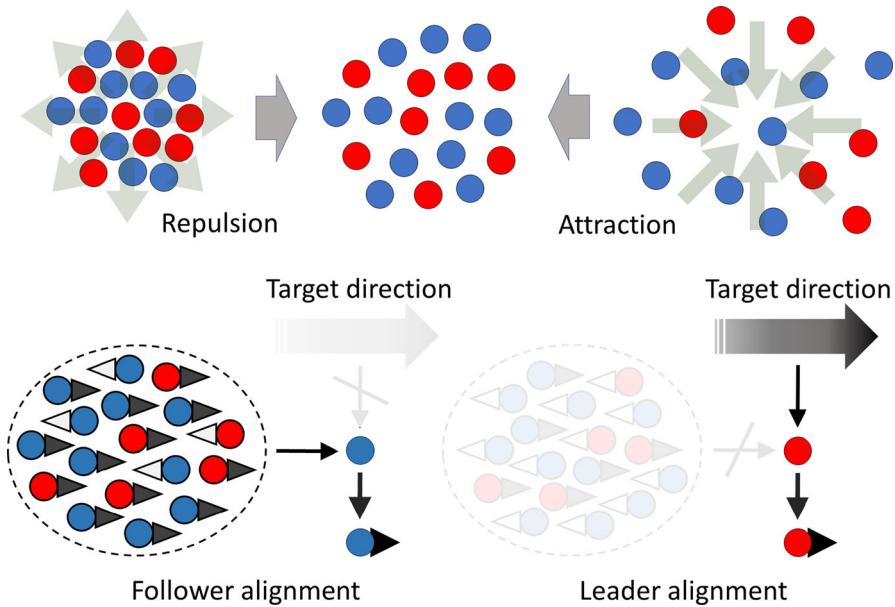
Fig. 1 Assumptions underlying the turning behaviour of swarm members. Top row: attraction and repulsion are assumed to act equally on followers (blue circles) and leaders (red circles). Repulsion acts over shorter ranges, pushing individuals away from each other if they are too close; attraction acts over larger distances, pulling individuals together if they become too separated. Bottom row: alignment is distinct for followers and leaders. Followers do not know the target but are influenced by the orientation of the oncoming swarm, reorienting when they perceive the oncoming swarm is moving in the opposite direction. Leaders ignore the alignment of the swarm, biasing instead according to the target direction (Color figure online)

The turning rate functions are non-local functions of $u^{\pm}$ and $v^{\pm}$ (the dependence will be specified shortly) and have the following form:

$$\lambda^{i\pm} = \lambda_1 + \lambda_2 f(y^{i\pm}), \tag{2}$$

for $i \in \{u, v\}$ and where

$$f(y) = 0.5 + 0.5 \tanh(y - y_0). \tag{3}$$

This assumes the turning rate smoothly and monotonically increases from a baseline to maximum value according to the level of *perceived signal*, measured separately for $(+)$ and $(-)$ follower and leader populations in $y^{u^{\pm}}$ and $y^{v^{\pm}}$. If y_0 is chosen in such a way that $f(0) \ll 1$, the coefficients λ_1 and λ_2 can be regarded as the *baseline turning rate* and the *highly biased turning rate*, respectively. For positively moving followers at position x and time t, $y^{u^+}(x, t)$ combines the repulsive, attractive and alignment interactions with their neighbours into a single measure that dictates the turning rate, with similar interpretations for y^{u^-}, $y^{v^{\pm}}$. Specifically, we set

$$y^{u\pm} = Q_r^{u\pm} + Q_a^{u\pm} + Q_l^{u\pm} \tag{4}$$

and similarly for $y^{v^{\pm}}$. If the resulting perceived signal $y^{i^{\pm}}$, for $i \in \{u, v\}$, is negative the agent will tend to continue moving in the same direction; otherwise, it will be more likely to turn. Q_r, Q_a and Q_l integrate the perceived positional and directional information from neighbours located at a distance $s \in (0, \infty)$ from the generic individual placed at (x, t).

For simplicity, we will assume here that followers and leaders are only distinguished by their alignment response: attraction/repulsion are taken as "universal" and act to keep the overall population together and avoid collisions. A noteworthy consequence of this is that a leader is not *bound* to choose the direction of the target: for example, if there is a danger of losing contact with the swarm the leader should be inclined to return to the fold. We adopt the following standard choices.

$$Q_r^{u^{\pm}} = Q_r^{v^{\pm}} = q_r \int_0^{\infty} K_r(s)\,(u(x \pm s) + v(x \pm s) - u(x \mp s) - v(x \mp s))\,\mathrm{d}s, \quad (5)$$

$$Q_a^{u^{\pm}} = Q_a^{v^{\pm}} = -q_a \int_0^{\infty} K_a(s)\,(u(x \pm s) + v(x \pm s) - u(x \mp s) - v(x \mp s))\,\mathrm{d}s. \tag{6}$$

In the above, $K_i(s)$, $i = \{a, r\}$, denote interaction kernels and parameters q_a and q_r represent the magnitude of the attraction and repulsion contributions, respectively. The attractive and repulsive terms depend on the total density of the cohort at a certain position, regardless of flight orientation, i.e. $u(x \pm s, t) = u^+(x \pm s, t) + u^-(x \pm s, t)$ and similarly $v(x \pm s, t) = v^+(x \pm s, t) + v^-(x \pm s, t)$. For an individual flying in the direction of a large swarm (i.e. towards overall higher total population densities), the contribution to y from Q_r will be positive (hence, an increased likelihood of turning away) and from Q_a will be negative (hence less likely to turn away). Whether the combined contribution is then positive or negative depends on the individual parameters and the precise shape of the total density distribution. As a further remark, it is instructive to note that expansions in s will generate, as local approximations, a dependency on the local gradient of the total density $u + v$ in each of the Q_r and Q_a functions. Under this, Q_a becomes large when moving down the gradient of $u + v$. This increases the rate of switching, and (in the absence of other interactions) there will be net movement towards high total densities. The reverse applies to Q_r.

The alignment contribution is of the general form

$$Q_l^{i^{\pm}} = q_l \int_0^{\infty} K_l(s) P^i\left(u^{\pm}, v^{\pm}\right)\mathrm{d}s, \tag{7}$$

for $i \in \{u, v\}$ and where $K_l(s)$ and q_l, respectively, denote the alignment kernel and the magnitude of the synchronisation. The functions $P^u(u^{\pm}, v^{\pm})$ and $P^v(u^{\pm}, v^{\pm})$, respectively, represent how the swarm influences alignment for the follower and leader populations. Choices for Q_l, i.e. the specification of $P^i(u^{\pm}, v^{\pm})$, form the point of distinction for various models and are described below, see Table 1 for a summary of the models interactions. As we see in Sect. 2.2, the latter may simply take into account a fixed preferred direction, i.e. modelling a case where a population knows where it wants to go.
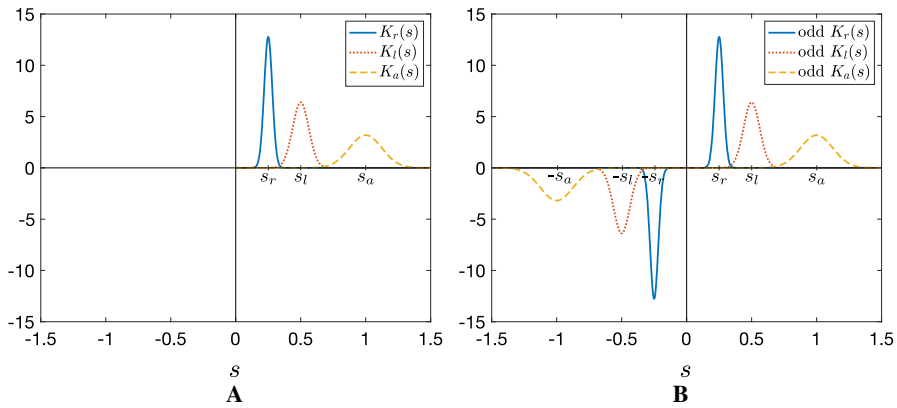
Fig. 2 Kernel functions. **a** Translated Gaussian kernels for repulsion, alignment, and attraction, described in Eq. (8). **b** Odd extension of translated Gaussian kernels to the whole real line for repulsion, alignment, and attraction. The interaction ranges satisfy the condition $s_r < s_l < s_a$

Interaction kernels are given by the following translated Gaussian functions

$$K_i(s) = \frac{1}{\sqrt{2\pi m_i^2}} \exp\left(\frac{-(s-s_i)^2}{2m_i^2}\right), \quad i = r, a, l \quad s \in [0, \infty), \tag{8}$$

where s_r, s_a, and s_l are half the length of the repulsion, attraction, and alignment ranges, respectively, see Fig. 2a. The constants m_i, $i = r, a, l$, are chosen to ensure $> 98\%$ of the support of the kernel mass falls inside $[0, \infty)$ (specifically, $m_i = \frac{s_i}{8}$, $i = r, a, l$). This allows a high-level approximation of the integral defined on $[0, \infty)$ to that defined on the whole real line.

2.1 Follower–Leader Model

The full follower–leader model assumes the following leader alignment

$$Q_l^{v\pm} = \mp 2q_l \int_0^\infty K_l(s)\varepsilon \, ds = \text{constant} \tag{9}$$

where we call ε the *orientation bias parameter*. Leaders ignore other swarm members for alignment, receiving instead a (spatially uniform and constant) alignment bias if the orientation bias is operating, i.e. if $\varepsilon > 0$. Invoking the honey bees example, scouts have generally agreed on the new nest at swarm take-off. Generalisations could include letting ε explicitly depend on a variable factor or including an influence of alignment from other swarm members.

Alignment of followers is taken to be

$$Q_l^{u\pm} = q_l \int_0^\infty K_l(s) \left(u^\mp(x \pm s) + \alpha_\mp v^\mp(x \pm s) - u^\pm(x \mp s) - \alpha_\pm v^\pm(x \mp s) \right) ds. \tag{10}$$

This dictates that a follower will be more likely to turn when it detects, within the region ahead of its direction of travel, a large number of individuals moving in the opposite direction. On the other hand, it will tend to keep the same direction if there are a large number of individuals moving in the same direction in the region to its rear. It is possible to consider other plausible forms and we choose the present form for its consistency with that assumed in Eftimie et al. (2007). Note that $\alpha_\pm$ are weighting parameters that distinctly weight the leader conspicuousness, **c-bias**. Completely inconspicuous leaders would correspond to $\alpha_\pm = 0$ while if leaders are completely indistinguishable from followers $\alpha_\pm = 1$. If leaders engage in behaviour that raises (lowers) their conspicuousness when flying towards (away from) the destination, we would choose $\alpha_+/\alpha_- > 1$ ($\alpha_+/\alpha_- < 1$). For bee swarms, streaking towards the nest by the scout leaders may serve to increase visibility, while "laying low" on return may decrease it (Seeley 2010).

2.2 Leaders-Only Model

A leaders-only model can be obtained from the full follower–leader model by setting follower populations to zero ($u^\pm(x, t) = 0$). As noted, attraction/repulsion social interactions are maintained, but the alignment bias is independent of the population. The target direction is potentially favoured through **o-bias** (ε) and **s-bias** ($\beta_+ \neq \beta_-$, differential speeds). The model reduces to

$$\begin{aligned} \frac{\partial v^+}{\partial t} + \beta_+ \frac{\partial v^+}{\partial x} &= -\lambda^{v^+} v^+ + \lambda^{v^-} v^-, \\ \frac{\partial v^-}{\partial t} - \beta_- \frac{\partial v^-}{\partial x} &= +\lambda^{v^+} v^+ - \lambda^{v^-} v^-, \\ v^\pm(x, 0) &= v_0^\pm(x), \end{aligned} \tag{11}$$

where

$$\lambda^{v\pm} = \lambda_1 + \lambda_2 \left[0.5 + 0.5 \tanh \left(y^{v\pm} - y_0 \right) \right], \quad \text{with } y^{v\pm} = Q_r^{v\pm} + Q_a^{v\pm} + Q_l^{v\pm}.$$

The interaction contributions derive from Eqs. (5), (6) and (9) are given by

$$Q_r^{v\pm} = q_r \int_0^\infty K_r(s) \left(v(x \pm s) - v(x \mp s) \right) ds, \tag{12}$$

$$Q_a^{v\pm} = -q_a \int_0^\infty K_a(s) \left(v(x \pm s) - v(x \mp s) \right) ds, \tag{13}$$

Table 1 Summary of the interactions involved in the models

Pop. composition	Full		LO	FO
	Leaders (L)	Followers (F)	Leaders (L)	Followers (F)
Attraction to	F + L	F + L	F + L	F + L
Repulsion to	F + L	F + L	F + L	F + L
Alignment to	Implicit orientation bias ε	F + L (weighted with $\alpha_\pm$)	Implicit orientation bias ε	F+ implicit leader bias η

"Full" denotes full follower-leader model; "LO" denotes leaders-only model; "FO" denotes followers-with-implicit-leaders model

$$Q_l^{v\pm} = \mp 2q_l \int_0^\infty K_l(s)\varepsilon \mathrm{d}s = \text{constant.} \tag{14}$$

2.3 Followers-with-Implicit-Leaders Model

We exclude explicit representation of leaders by ignoring their dynamic evolution. Specifically, we stipulate fixed and uniform leader populations, i.e. $v^+(x,t)$ and $v^-(x,t)$ are constant in space and time. A leader contribution to attraction and repulsion is eliminated while their contribution to follower alignment is reduced to a fixed and constant bias, which we refer to as an *implicit leader bias* and represent by parameter η: large η corresponds to highly influential leaders. The resulting model is given by

$$\frac{\partial u^+}{\partial t} + \gamma \frac{\partial u^+}{\partial x} = -\lambda^{u^+} u^+ + \lambda^{u^-} u^-,$$
$$\frac{\partial u^-}{\partial t} - \gamma \frac{\partial u^-}{\partial x} = +\lambda^{u^+} u^+ - \lambda^{u^-} u^-,$$
$$u^\pm(x,0) = u_0^\pm(x), \tag{15}$$

where

$$\lambda^{u^\pm} = \lambda_1 + \lambda_2 \left[0.5 + 0.5 \tanh(y^{u^\pm} - y_0) \right], \quad \text{with } y^{u^\pm} = Q_r^{u^\pm} + Q_a^{u^\pm} + Q_l^{u^\pm}.$$

and interaction terms

$$Q_r^{u^\pm} = q_r \int_0^\infty K_r(s) \left(u(x \pm s) - u(x \mp s) \right) \mathrm{d}s, \tag{16}$$

$$Q_a^{u^\pm} = -q_a \int_0^\infty K_a(s) \left(u(x \pm s) - u(x \mp s) \right) \mathrm{d}s, \tag{17}$$

$$Q_l^{u^\pm} = q_l \int_0^\infty K_l(s) \left(u^\mp(x \pm s) - u^\pm(x \mp s) \mp \eta \right) \mathrm{d}s. \tag{18}$$

Table 2 Table of parameters varied throughout this study

Grouping	Parameter	Description	Model
Bias:	α_+	Alignment due to $(+)$ oriented leaders	Full
	α_-	Alignment due to $(-)$ oriented leaders	Full
	η	Implicit leader bias	FO
	ε	Implicit orientation bias	LO, Full
	β_+	Speed of $(+)$ moving leaders	LO, Full
	β_-	Speed of $(-)$ moving leaders	LO, Full
Pop. size:	A_u	Mean follower density	FO, Full
	A_v	Mean leader density	LO, Full
	M_u	Maximum initial follower density	Full
	M_v	Maximum initial leader density	Full
Interaction:	q_r	Repulsion strength	All
	q_l	Alignment strength	All
	q_a	Attraction strength	All
Others:	λ_1	Baseline turning rate	All
	λ_2	Bias turning rate	All

The parameters that are fixed throughout this study are summarised in Table 3 (see Appendix B)."Full" denotes full follower-leader model; "LO" denotes leaders-only model; "FO" denotes followers-with-implicit leaders model

2.4 Parameters

Given its complexity, the model has a large parameter set and we therefore fix many at standard values, based on previous studies (Eftimie et al. 2007) and listed in Appendix B. The fixed parameters include the follower speed γ as well as the inter-action ranges s_r, s_l, s_a, fixed to generate "short-range repulsion, mid-range alignment and long-range attraction", a common assumption in biological models of swarming behaviour (Sumpter 2010; Carrillo et al. 2010; Fetecau and Guo 2012). Similarly, the more technical parameters y_0, m_l, m_a, m_r are also chosen according to Eftimie et al. (2007), see Appendix B.

Consequently, we focus on a smaller set of key parameters that distinguish leader/follower movement, listed in Table 2 along with the models to which they belong. In particular, we highlight the *bias* parameters that stipulate a level of attempted leader influence. We also remark that model formulations lead to conservation of follower and leader populations, generating two further population size parameters A_u and A_v, denoting the mean total follower and leader densities. Related to these are the parameters M_u and M_v, denoting the maximum initial follower and leader densities, respectively, and employed in the definition of certain initial conditions for the model in Sect. 4. As a final note, we generally restrict to alignment-attractive dominated regimes, i.e. q_a, $q_l \gg q_r$.

3 Dynamics of Reduced Models

We first analyse the dynamics of the simplified models, via linear stability analysis and numerical simulation. Note that details of the numerical scheme are provided in Appendix C.

3.1 Leaders-Only Model

In this model, all swarm members have some knowledge of their target and bias their movement through two mechanisms: **o-bias**, orientation according to the target and parametrised by $\varepsilon \geq 0$, and **s-bias**, differential speed of movement, i.e. $\beta_+ \geq \beta_-$.

3.1.1 Steady States and Stability Analysis

We first examine the form and stability of spatially homogeneous steady state (HSS) solutions, $v^+(x, t) = v^*$ and $v^-(x, t) = v^{**}$, for the leaders-only model (11–14). Conservation of mass leads to $A_v = v^* + v^{**}$, where A_v is the sum of initial population densities averaged over space ($A_v = \langle v_0^+(x) + v_0^-(x) \rangle$). The steady-state equation is obtained by solving

$$h(v^*, q_l, \lambda, A_v, \varepsilon) = 0, \tag{19}$$

where

$$\begin{aligned} h\left(v^*, q_l, \lambda, A_v, \varepsilon\right) &= -v^*(1 + \lambda \tanh(-2\varepsilon q_l - y_0)) \\ &\quad + \left(A_v - v^*\right)(1 + \lambda \tanh(2\varepsilon q_l - y_0)) \end{aligned} \tag{20}$$

and

$$\lambda = \frac{0.5\lambda_2}{0.5\lambda_2 + \lambda_1}. \tag{21}$$

From Eq. 19, we obtain a single HSS solution

$$v^* = \frac{A_v \left[1 + \lambda \tanh(2\varepsilon q_l - y_0)\right]}{2 + \lambda \tanh(-2\varepsilon q_l - y_0) + \lambda \tanh(2\varepsilon q_l - y_0)}. \tag{22}$$

For $q_l = 0$ (no alignment) or $\varepsilon = 0$ (no **o-bias**), we obtain an *unaligned* HSS $(v^*, v^{**}) = \left(\frac{A_v}{2}, \frac{A_v}{2}\right)$, i.e. a population equally distributed into those moving in ($\pm$) directions. Assuming $\varepsilon > 0$, dominating alignment ($q_l \to \infty$) leads to steady state $(v^*, v^{**}) = (A_v(1 + \lambda)/2, A_v(1 - \lambda)/2)$. For $q_l > 0$ the same result follows for dominating **o-bias**, i.e. $\varepsilon \to \infty$. Intuitively, the introduction of bias eliminates symmetry, with $\varepsilon > 0$ tipping the balance into a ($+$) direction, with alignment amplifying the effect. The steady-state variation with ε is illustrated in Fig. 3a. Unlike **o-bias**,

introduction of differential leader speed does not alter the HSS solution, since h does not depend on $\beta_{\pm}$, see Fig. 3b.

To assess stability and the potential for pattern formation we perform a standard linear stability analysis. Specifically, we examine the growth from homogeneous and inhomogeneous perturbations of the HSS at $(v^*, v^{**}) = (v^*, A_v - v^*)$. Note that, extending K_r and K_a to odd kernels on the whole real line, see Fig. 2b, Eqs. (12) and (13) can be rewritten as

$$Q_r^{v\pm} = q_r \int_{-\infty}^{+\infty} K_r(s)v(x \pm s)\mathrm{d}s, \tag{23}$$

$$Q_a^{v\pm} = -q_a \int_{-\infty}^{+\infty} K_a(s)v(x \pm s)\mathrm{d}s. \tag{24}$$

We set $v^+(x,t) = v^* + v_p(x,t)$ and $v^-(x,t) = v^{**} + v_m(x,t)$, where $v_p(x,t)$ and $v_m(x,t)$ each denote small perturbations. We substitute into (11), neglect nonlinear terms in v_p and v_m and look for solutions $v_{p,m} \propto e^{\sigma t + ikx}$. Here, k is referred to the wavenumber (or spatial eigenvalue) while σ is the growth rate (or temporal eigenvalue). A few rearrangements lead to the expression

$$\sigma^+(k) = \frac{C(k) + \sqrt{C(k)^2 - D(k)}}{2}, \tag{25}$$

where $\sigma^+(k)$ is used to denote the growth rate with largest real part. In the above

$$C(k) = (\beta_- - \beta_+)ik - 2\lambda_1 - \lambda_2 - 0.5\lambda_2 \left[\tanh(-2q_l\varepsilon - y_0) + \tanh(2q_l\varepsilon - y_0)\right],$$
$$D(k) = 4\beta_+\beta_- k^2 + 4ik\lambda_1(\beta_+ - \beta_-) \tag{26}$$
$$+ 2\lambda_2 ik \left\{ \beta_+(1 + \tanh(2q_l\varepsilon - y_0)) - \beta_-(1 + \tanh(-2q_l\varepsilon - y_0)) \right.$$
$$+ v^* \left[1 - \tanh^2(-2q_l\varepsilon - y_0)\right] \left[\left(-q_r \hat{K}_r^+(k) + q_a \hat{K}_a^+(k)\right)(\beta_+ + \beta_-)\right]$$
$$+ v^{**} \left[1 - \tanh^2(2q_l\varepsilon - y_0)\right] \left[\left(q_r \hat{K}_r^-(k) - q_a \hat{K}_a^-(k)\right)(\beta_+ + \beta_-)\right] \right\}, \tag{27}$$

where $\hat{K}_j^{\pm}(k)$, $j = r, a, l$ denote the Fourier transform of the kernel $K_j(s)$, i.e.

$$\hat{K}_j^{\pm}(k) = \int_{-\infty}^{+\infty} K_j(s)e^{\pm iks}\mathrm{d}s = \exp\left(\pm i s_j k - \frac{k^2 m_l^2}{2}\right), \quad j = r, a, l. \tag{28}$$

The HSS is unstable (stable) to homogeneous perturbations if $\Re(\sigma^+(0)) > 0$ ($\Re(\sigma^+(0)) \leq 0$) and unstable to inhomogeneous perturbations if $\Re(\sigma^+(k)) > 0$ for at least one valid $k > 0$ (for an infinite domain, we simply require $\Re(\sigma^+(k)) > 0$ for at least one value of $k \in \mathbb{R}^+$). Any k for which $\Re(\sigma^+(k)) > 0$ is referred to as an unstable wavenumber.

We classify HSS stability according to the following principle forms:

(U) Unstable to homogeneous perturbations, i.e. $\Re(\sigma^+(0)) > 0$. Solutions are expected to diverge from the HSS both with and without movements.

(S) Stable to homogeneous and inhomogeneous perturbations, i.e. $\Re(\sigma^+(k)) < 0, \quad \forall k \geq 0$. We expect small (homogeneous or inhomogeneous) perturbations to decay and solutions that evolve to the HSS.

(SP) Stationary patterns, HSS stable to homogeneous perturbations and unstable to inhomogeneous perturbations. Specifically, we have $\Re(\sigma^+(0)) \leq 0$ but $\exists \tilde{k} > 0 : \Re(\sigma^+(\tilde{k})) > 0$ where, for any such $\tilde{k}$, $\Im(\sigma^+(\tilde{k})) = 0$.

(DP) Dynamic patterns, as (SP), but $\Im(\sigma^+(\tilde{k})) \neq 0$ for at least some of the unstable wavenumbers.

(SP) and (DP) both indicate a Turing-type instability (Turing 1952), i.e. symmetry breaking in which a spatial pattern emerges from quasi-homogeneous initial conditions. The presence of wavenumbers where $\Im(\sigma^+(\tilde{k})) \neq 0$ implies growing patterns that oscillate in both space and time, potentially generating a dynamic pattern (e.g. a travelling swarm). These are, though, predictions based on solutions to the linearised system and nonlinear dynamics are likely to introduce further complexity.

Key results from the analysis are summarised in Fig. 3, indicating that both the HSS and its stability change with bias parameters ε (or q_l), the ratio β_+/β_- and q_a. As noted above, increasing ε (or q_l) generates a HSS with $(\pm)$ distributions increasingly favouring the target direction. Variations in the β_+/β_- ratio do not alter the HSS value but do impact on the stability. Under both o-bias and s-bias, the stability nature changes at key threshold values, critically depending on the strength of attraction, q_a. For low q_a the HSS is stable for all values of ε and/or β_+/β_-: attraction is insufficient to cluster the population and it remains dispersed (result not shown). There may be biased movement towards the target, but the population remains in a uniformly dispersed/non-swarming state.

For larger q_a, however, the HSS becomes unstable under inhomogeneous perturbations. A Turing-type instability occurs and emergence of a spatial pattern is expected. Specifically, the key threshold value increases for larger q_a (compare top and bottom panels of Fig. 3a and b). The predicted pattern critically depends on the bias. For an unbiased scenario ($\varepsilon = 0$ and $\beta_+/\beta_- = 1$) we have stability class (SP) and predict a stationary pattern, see orange asterisks in Fig. 3a and b. Simulations corroborate this prediction (see Fig. 3c), where we observe stationary cluster formation. Each cluster is weighted equally between $(\pm)$ directed populations and the overall cluster is fixed in position. Note, however, that the nonlocal elements of the model generate a degree of intercluster communication and, over longer timescales, clusters may attract each other and merge.

Introducing **o-bias** ($\varepsilon > 0$) or **s-bias** ($\beta_+/\beta_- > 1$), though, generates growth rates with imaginary components—this follows from the nonzero imaginary parts of $D(k)$ and/or $C(k)$—and the instability is of type (DP). In this case a dynamic component is predicted, with simulations substantiating this, cf. Fig. 3d and e. The forming clusters are asymmetrically distributed between $(\pm)$ directed movement and, overall, we observe steered swarming: clusters move in the direction determined by the bias. Notably, clusters move at distinct speeds according to their size, so that clusters collide and merge. Eventually, a single steered swarm has formed and migrates with
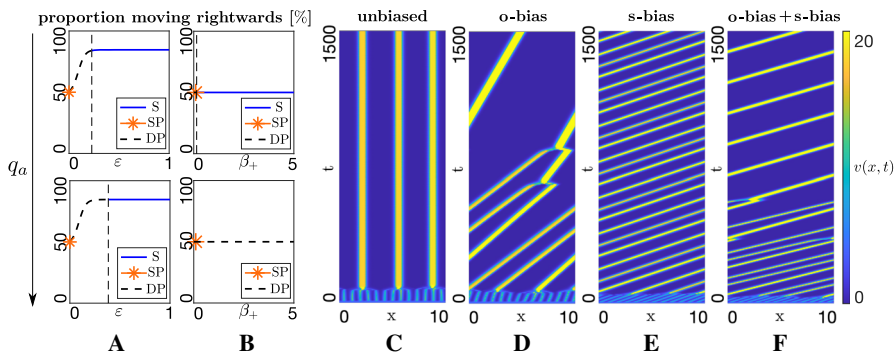
Fig. 3 Dynamics of the leaders-only model. **a–b** Bifurcation plots showing HSS (proportion moving right-wards) and stability under parameter variation. **a** O-bias, i.e. variation of ε under low (top panel, $q_a = 0.5$) and high (bottom panel, $q_a = 50$) attraction (s-bias inactive, $\beta_+ = \beta_- = 0.1$). **b** S-bias, varying β_+ for fixed $\beta_- = 0.1$, under low (top panel, $q_a = 0.5$) and high (bottom panel, $q_a = 50$) attraction (o-bias inactive, $\varepsilon = 0$). Solid blue and dashed black lines denote stability class (S) and (DP), respectively, orange asterisks indicate stability class (SP). **c–f** Space–time density map showing evolving total leader density, under: **c** unbiased case (o-bias and s-bias inactive, $\varepsilon = 0, \beta_+ = \beta_- = 0.1$), generating a stationary patterns; **d** o-bias, obtained for $\varepsilon = 0.2$ (s-bias inactive, $\beta_+ = \beta_- = 0.1$), generating target directed swarms; **e** s-bias, obtained for $\beta_+/\beta_- = 0.2/0.1$ (o-bias inactive, $\varepsilon = 0$), generating target directed swarms; **f** o-bias and s-bias, obtained for $\varepsilon = 0.2$ and $\beta_+/\beta_- = 0.2/0.1$, generating target directed swarms with enhanced speed. **c–f** ICs are perturbations of $(v^*, v^{**}) = (2, 2)$. **d** ICs are perturbations of $(v^*, v^{**}) = (3.329, 0.671)$. In all plots, other parameters are set at $q_r = 0.1, q_l = 7.5$, (**c–f** $q_a = 7.5$), $A_v = 4, \lambda_1 = 0.2, \lambda_2 = 0.9$ (Color figure online)

fixed speed and shape (a travelling pulse). The simultaneous action of o-bias and s-bias generates similar behaviour, Fig. 3f, with the combined action creating faster movement towards the target.

Summarising, the leaders-only model illustrates the distinct contributions from different model elements: (i) attraction is crucial to aggregate a dispersed population; (ii) assuming sufficient attraction, either **o-bias** or **s-bias** is sufficient to propel the swarm in the direction of the target, with increased swarm speed if both biases act together.

3.2 Followers-with-Implicit-Leaders Model

We next examine the followers-with-implicit-leaders model. Interaction occurs through attraction, repulsion and alignment, with an additional uniform alignment bias parametrised by η and corresponding to implicit perception of a leader population.

3.2.1 Steady States and Stability Analysis

Proceeding as before, we explore the form of spatially homogeneous steady state solutions. Conservation of the total follower population leads to $A_u = u^* + u^{**}$, where A_u is the average (over space) of the sum of initial population densities, $A_u =$

$\langle u_0^+(x) + u_0^-(x) \rangle$. Steady states will be given by

$$h(u^*, q_l, \lambda, A_u, \eta) = 0, \tag{29}$$

where

$$\begin{aligned} h\left(u^*, q_l, \lambda, A_u, \eta\right) = & -u^* \left(1 + \lambda \tanh(A_u q_l - 2u^* q_l - \eta q_l - y_0)\right) \\ & + \left(A_u - u^*\right)\left(1 + \lambda \tanh(-A_u q_l + 2u^* q_l + \eta q_l - y_0)\right) \end{aligned} \tag{30}$$

and

$$\lambda = \frac{0.5\lambda_2}{0.5\lambda_2 + \lambda_1}. \tag{31}$$

The zero-bias scenario ($\eta = 0$) has been analysed in depth previously, see Eftimie et al. (2007), and we restrict to a brief summary. First, a single *unaligned* HSS exists at

$$\left(u^*, u^{**}\right) = \left(\frac{A_u}{2}, \frac{A_u}{2}\right), \tag{32}$$

i.e. both directions equally favoured. Dominating alignment ($q_l \to \infty$) generates two further HSS at $(u^*, u^{**}) = (A_u(1 \mp \lambda)/2, A_u(1 \pm \lambda)/2)$: each *aligned* HSS corresponds to a population where alignment induces the population to favour one direction. A typical structure for the bifurcation diagram is illustrated in Fig. 4a: a central branch corresponding to the unaligned HSS and upper and lower aligned branches. For the chosen parameters, these branches are connected via a further set of intermediate (unstable) branches. Thus, as q_l increases the number of steady states shifts between 1, 5 and 3 steady states (see also Fig. 11 of Appendix D.2).

The symmetric structure of $\eta = 0$ is lost for $\eta \neq 0$, even under small values: see Fig. 4b–c. The aligned HSS branch corresponding to the target direction is more likely to be selected, the other branch is shifted rightwards (Fig. 4b) and for larger η disappears entirely (Fig. 4c). Overall, the external bias is amplified by follower to follower alignment and the population becomes predominantly oriented in the target direction.

We extend to a spatial linear stability analysis, applying the same process as in Sect. 3.1.1 to obtain the following dispersion relation

$$\sigma^+(k) = \frac{C(k) + \sqrt{C(k)^2 - D(k)}}{2}, \tag{33}$$

where

$$\begin{aligned} C(k) &= \left(\lambda_{u-}^{u+} - \lambda_{u+}^{u+}\right) u^+ + \left(\lambda_{u+}^{u-} - \lambda_{u-}^{u-}\right) u^- - \lambda^{u-} - \lambda^{u+}, \\ D(k) &= 4\gamma^2 k^2 \end{aligned} \tag{34}$$
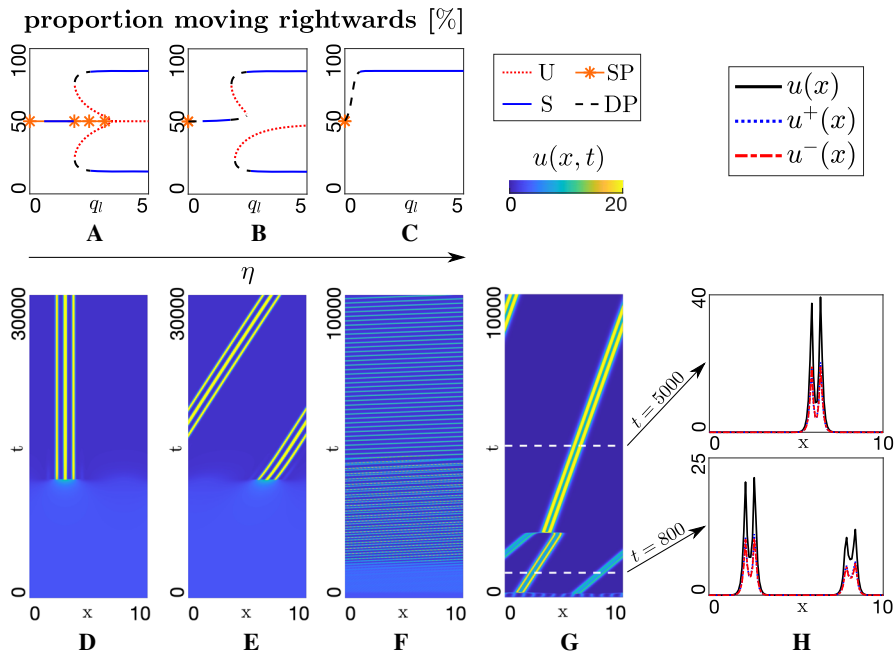
Fig. 4 Dynamics of the followers-with-implicit-leaders model. **a–c** Bifurcation plots showing HSS (proportion moving rightwards) and stability under parameter variation. Bifurcation parameter is q_l and the resulting bifurcation plots are shown for **a** $\eta = 0$ (unbiased), **b** $\eta = 0.04$, **c** $\eta = 4$. Other parameters set at $q_r = 0$, $q_a = 0.25$, $A_u = 2$, $\lambda_1 = 0.8$, $\lambda_2 = 3.6$. Stability classes plotted as (U): dotted red, (S): solid blue, (SP): orange asterisks, (DP): dashed black. **d–f** Space–time plot showing the evolving total follower density under variation of η: **d** $\eta = 0$ (unbiased), **e** $\eta = 0.04$, **f** $\eta = 4$. Stronger biases lead to faster swarm movement towards the target. Other parameters set as in **a–c** with $q_l = 0.4$. ICs are perturbations of $(u^*, u^{**}) = (1, 1)$. In **g–h**, we demonstrate the merging of faster and slower swarms, under the parameter set $\eta = 0.4$, $q_r = 0.1$, $q_l = 1$, $q_a = 10$, $A_u = 2$, $\lambda_1 = 0.2$, $\lambda_2 = 0.9$ (Color figure online)

$$+4\gamma i k \left[\left(-\lambda_{u^-}^{u^+} - \lambda_{u^+}^{u^+} \right) u^+ + \left(\lambda_{u^-}^{u^-} + \lambda_{u^+}^{u^-} \right) u^- + \lambda^{u^-} - \lambda^{u^+} \right]. \quad (35)$$

In the above, $\lambda_{u^\pm}^{u^\pm}$ denote the partial derivatives of $\lambda^{u^\pm}$ with respect to $u^\pm$ and subsequently evaluated at the HSS (u^*, u^{**}). We note that these are functions of k, though we have suppressed this dependency for compactness. For reference, we provide the explicit forms in Appendix D.1, yet intricacy of the dispersion relation restricts us to a numerical approach. Stability is again classified into one of the 4 classes described earlier.

The diagrams shown in Fig. 4a–c reveal a complex bifurcation structure and potentially diverse dynamics according to parameter selection and initial condition. Indeed, this has already been highlighted in depth for the unbiased ($\eta = 0$) model in Eftimie et al. (2007), where various complex spatiotemporal pattern forms have been revealed. For example, Fig. 12 in Appendix D.3 illustrates transitioning between stationary and dynamic aggregates as the key parameter q_l is altered. Note that moving aggregates

can be generated without any incorporated bias, though if the population begins quasi-symmetric either direction will be selected with equal likelihood.

Here we focus on the extent to which introduction of a bias influences the dynamics of aggregate structures, with Fig. 4d–g providing a representative sequence. We begin with an unbiased scenario, setting $\eta = 0$ and choosing parameters from a region predicted to lead to stationary patterning. We initiate populations in quasi-symmetric fashion, setting

$$u^+(x, 0) = \frac{A_u\,(1 + r_u(x))}{2}, \quad u^-(x, 0) = \frac{A_u\,(1 - r_u(x))}{2}, \tag{36}$$

where $r_u(x)$ denotes a small random perturbation. As expected from the stability analysis, a stationary cluster forms (see Fig. 4d) with its shape and position maintained by a symmetric distribution of ($\pm$) directed populations. Introducing bias, though, disrupts the symmetry and Turing instabilities falls into the dynamic pattern class. Moreover, even a marginal alignment bias strongly selects clusters that move in the direction of the bias, e.g. see Fig. 4e. Starting from a symmetric or nonaligned initial set-up, bias slightly tilts followers towards the target. Follower–follower alignment snowballs, eventually resulting in a cluster moving towards the target. Increasing the bias magnitude increases swarm speed, Fig. 4f.

As in the leaders-only model, there is a clear relationship between cluster speed and cluster size. This is illustrated in Fig. 4g, where the initial symmetry breaking process generates two clusters of slightly different size, Fig. 4h (bottom). Both clusters move in the target direction, but the smaller cluster is considerably faster. The clusters eventually collide and merge to form an even larger and slower cluster, see Fig. 4h (top). Note that, in principle it is also possible to obtain a swarm migrating against the target direction, e.g. by heavily favouring biasing the initial conditions. Simulations, though, suggest that such situations are highly unlikely to occur in practice.

Introducing bias can even trigger symmetry breaking, as shown in Fig. 5. To highlight this, we neglect attractive and repulsive interactions ($q_a = q_r = 0$) and focus solely on alignment. Initially setting $\eta = 0$, remaining parameters are specified such that the unaligned HSS (i.e. $u^* = u^{**}$) is stable to both homogeneous and inhomogeneous perturbations: a typical dispersion relation is provided in Fig. 5a (top), showing the absence of wavenumbers with positive growth rates and the corresponding simulation confirms the absence of pattern formation, Fig. 5b. Introducing bias ($\eta > 0$) breaks symmetry, yielding a nonzero range of wavenumbers with positive growth rates, Fig. 5a (bottom). A pattern emerges which generates multiple clusters moving in the target direction, Fig. 5c.

Summarising the analysis and numerics in this section, we emphasise that the followers-with-implicit-leaders submodel can display a range of aggregating/swarming behaviour, where the processes of alignment and attraction combine to generate one or more cluster. The addition of bias breaks directional symmetry, eliminating the formation of stationary structures and generating clusters that move coherently in the target direction.
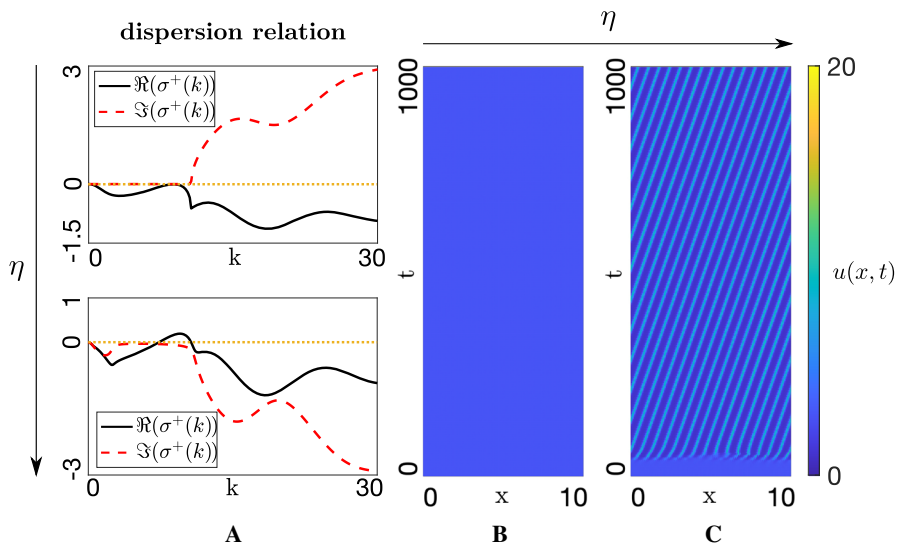
Fig. 5 **a** Dispersion relations and **b**–**c** the corresponding numerical simulations for the following parameter values: $q_r = 0$, $q_l = 2.1$, $q_a = 0$, $A_u = 2$, $\lambda_1 = 0.8$, $\lambda_2 = 3.6$. **a** Top row and **b** assume no bias ($\eta = 0$), while **a** bottom row and **c** consider the effect of a small alignment bias ($\eta = 0.08$). **b**–**c** ICs are perturbations of $(u^*, u^{**}) = (1,1)$

4 Dynamics of the Full Follower–Leader Model

We turn attention to the full "follower–leader" model, formed from Eqs. (1–10) and where followers constitute a completely naive population. Our principal aim will be to understand whether a steered swarm can arise under leader generated bias. Relying principally on numerical solution of the PDEs, we focus on two general parameter regimes: (P1) strong attraction–strong alignment, and (P2) strong attraction–weak alignment. For simplicity we neglect repelling interactions ($q_r = 0$). A bias corresponding to the (+)-direction can occur through parameter choices:

– **O-bias**, $\varepsilon > 0$, orientation;
– **S-bias**, $\beta_+ > \beta_-$, speed;
– **C-bias**, $\alpha_+ > \alpha_-$, conspicuousness.

Consequently, the *unbiased case* is $\varepsilon = 0$, $\alpha_+ = \alpha_-$, and $\beta_+ = \beta_-$. As discussed earlier, evidence is found for each bias in our honey bee swarming exemplar. Note that parameter regimes are selected such that linear stability analysis of the uniform solution in the unbiased case predicts Turing pattern formation.

4.1 Steady-State Analysis

Steady-state analysis proceeds as before: we look for the spatially homogeneous steady states $u^+(x, t) = u^*$, $u^-(x, t) = u^{**}$ and $v^+(x, t) = v^*$ and $v^-(x, t) = v^{**}$, noting that conservation ensures $A_u = u^* + u^{**}$ and $A_v = v^* + v^{**}$, where A_u and A_v are as

earlier described. Steady states for the full model satisfy

$$h_u\left(u^*, q_l, \lambda, A_u, A_v, \alpha_-, \alpha_+, y_0\right) = 0, \tag{37}$$

$$h_v\left(v^*, q_l, \lambda, A_v, \varepsilon, y_0\right) = 0, \tag{38}$$

where

$$
\begin{aligned}
h_u &= -u^*\left(1 + \lambda \tanh\left(A_u q_l - 2u^* q_l + q_l \alpha_-\left(A_v - v^*\right) - q_l \alpha_+ v^* - y_0\right)\right) \\
&\quad + \left(A_u - u^*\right)\left(1 + \lambda \tanh\left(-A_u q_l + 2u^* q_l + q_l \alpha_+ v^* - q_l \alpha_-\left(A_v - v^*\right) - y_0\right)\right), \\
h_v &= -v^*\left(1 + \lambda \tanh\left(-2\varepsilon q_l - y_0\right)\right) + \left(A_v - v^*\right)\left(1 + \lambda \tanh(2\varepsilon q_l - y_0)\right),
\end{aligned}
$$

and

$$\lambda = \frac{0.5\lambda_2}{0.5\lambda_2 + \lambda_1}. \tag{39}$$

Leader steady states correspond to those obtained previously for the leaders-only model. Hence, the proportion of leaders at HSS moving in the (+) direction increases monotonically between $A_v/2$ and $A_v(1 + \lambda)/2$, according to ε and/or q_l, (Fig. 3a). This equivalence stems from the simplification that leaders ignore others with respect to alignment.

In absence of alignment, i.e. $q_l = 0$, we find a single unaligned HSS at $(u^*, u^{**}, v^*, v^{**}) = (A_u/2, A_u/2, A_v/2, A_v/2)$. If $q_l \neq 0$, follower steady states are clearly more complex and we first consider the unbiased case ($\varepsilon = 0, \alpha_+ = \alpha_-,$ $\beta_+ = \beta_-$). Here we have $v^* = v^{**} = A_v/2$ and hence

$$
\begin{aligned}
h_u &= -u^*\left(1 + \lambda \tan\left(A_u q_l - 2u^* q_l - y_0\right)\right) \\
&\quad + \left(A_u - u^*\right)\left(1 + \lambda \tanh\left(-A_u q_l + 2u^* q_l - y_0\right)\right). \tag{40}
\end{aligned}
$$

Leaders have no influence and follower steady states are as observed for the followers-with-implicit-leaders model with $\eta = 0$. As described earlier, the number of follower steady states varies between 1, 3 and 5 (see Fig. 11 of Appendix D.2) with sufficiently large alignment allowing followers to self-organise into a dominating orientation.

We next consider an extreme **o-bias** ($\varepsilon \to \infty$), while excluding other biases ($\alpha = \alpha_+ = \alpha_-, \beta_+ = \beta_-$). Leaders favour the (+) direction, specifically $(v^*, v^{**}) = (\frac{A_v(1+\lambda)}{2}, \frac{A_v(1-\lambda)}{2})$, and hence

$$
\begin{aligned}
h_u &= -u^*\left(1 + \lambda \tanh\left(A_u q_l - 2u^* q_l - q_l \alpha A_v \lambda - y_0\right)\right) \\
&\quad + \left(A_u - u^*\right)\left(1 + \lambda \tanh\left(-A_u q_l + 2u^* q_l + q_l \alpha A_v \lambda - y_0\right)\right). \tag{41}
\end{aligned}
$$

The above has the same structure as for the followers-with-implicit-leaders model under external bias, where η in Eq. (29) is replaced by $\alpha A_v \lambda$. Consequently, for either increasing leader to follower influence (α) or increasing leader population size (A_v), bifurcations occur as in Fig. 4a–c: symmetric follower steady states become asymmetric, favoured according to the bias.
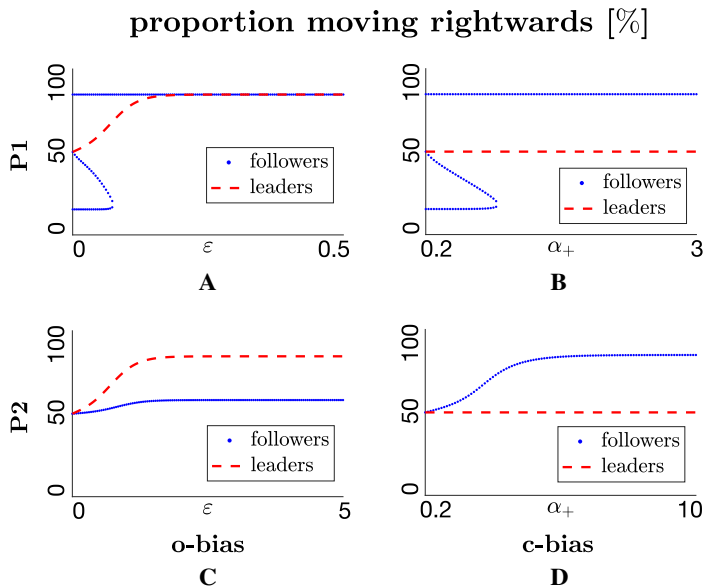
Fig. 6 Proportion of right-moving populations at steady state(s). **a**, **c** Effect of o-bias, increasing ε, on position and number of equilibrium points (s-bias and c-bias inactive, $\beta_- = \beta_+ = 0.1, \alpha_- = \alpha_+ = 1$). **b**, **d** Effect of c-bias, increasing α_+/α_-, on position and number of equilibrium points, for $\alpha_- = 0.2$ (o-bias and s-bias inactive, $\varepsilon = 0$ and $\beta_- = \beta_+ = 0.1$). Top row corresponds to (P1) strong attraction–strong alignment ($q_r = 0, q_l = 10, q_a = 8$), bottom row corresponds to (P2) strong attraction–weak alignment ($q_r = 0, q_l = 1, q_a = 10$). Other parameter values fixed at $A_u = A_v = 1, \lambda_1 = 0.2, \lambda_2 = 0.9$

Differential speeds (s-bias, $\beta_+ \neq \beta_-$) do not impact on steady states and we turn instead to distinct conspicuousness, specifically extreme **c-bias** ($\alpha_+/\alpha_- \to \infty$) while eliminating **o-bias**. Leader steady states remain symmetrical ($v^* = v^{**} = A_v/2$), yet distinct conspicuousness tips the majority of followers to the bias direction and a single steady state occurs at

$$\left(u^*, u^{**}, v^*, v^{**}\right) = (A_u(1 + \lambda)/2, A_u(1 - \lambda)/2, A_v/2, A_v/2). \qquad (42)$$

The bifurcation diagrams in Fig. 6 numerically confirm these results. Finally, we note that as $q_l \to \infty$ two further HSS's arise at $(u^*, u^{**}, v^*, v^{**}) = (A_u(1 \mp \lambda)/2, A_u(1 \pm \lambda)/2, A_v(1 + \lambda)/2, A_v(1 - \lambda)/2)$.

4.2 Numerical Simulation

The steady-state analysis provides insight into whether different biases induce left-right asymmetry, yet the emerging dynamics of spatial structures remains unclear. We numerically explore the full spatial nonlinear problem, in particular its capacity to generate a steered swarm as described earlier. Simulations will be conducted for two forms of initial condition.

(IC1) *Unbiased and dispersed.* Populations quasi-uniformly distributed in space and orientation. Letting A_u and A_v, respectively, denote the mean total follower and leader densities,

$$u^+(x,0) = \frac{A_u\,(1 + r_u(x))}{2}, \quad u^-(x,0) = \frac{A_u\,(1 - r_u(x))}{2},$$
$$v^+(x,0) = \frac{A_v\,(1 + r_v(x))}{2}, \quad v^-(x,0) = \frac{A_v\,(1 - r_v(x))}{2}. \tag{43}$$

(IC2) *Unbiased and aggregated.* Populations initially aggregated but unbiased in orientation. Letting M_u and M_v, respectively, denote the maximum initial follower and leader densities,

$$u^+(x,0) = \frac{M_u e^{-5(x-x_0)^2}\,(1 + r_u(x))}{2}, \quad u^-(x,0) = \frac{M_u e^{-5(x-x_0)^2}\,(1 - r_u(x))}{2},$$
$$v^+(x,0) = \frac{M_v e^{-5(x-x_0)^2}\,(1 + r_v(x))}{2}, \quad v^-(x,0) = \frac{M_v e^{-5(x-x_0)^2}\,(1 - r_v(x))}{2}. \tag{44}$$

Note that $r_u(x), r_v(x)$ denote small (1%) random perturbations. (IC1) allow investigation into whether dispersed populations self-organise into swarms while (IC2) tests whether aggregated populations maintain a swarm profile. (IC2) are particularly appropriate for bee swarming, where followers and leader scouts are initially clustered together.

4.2.1 Unbiased Dynamics

We first explore the capacity for self-organisation in the unbiased scenario. Note that each of the two principal parameter sets was selected to generate Turing instabilities and Fig. 7a and c demonstrates the patterning process under (P1) strong attraction–strong alignment and (P2) strong attraction–weak alignment, respectively. We observe the formation of multiple swarms which, in the absence of bias, remain in more or less fixed positions. Note, though, that over longer timescales inter-aggregate interactions may lead to drifting and merging. The arrangement and behaviour of an isolated swarm are investigated by initially aggregating the populations as in (IC2), with reorganisation leading to a stable and stationary swarm configuration and computed swarm wavespeed $c = 0$, Fig. 7b and d. Swarms contain leaders[1] concentrated at the swarm centre, with followers symmetrically dispersed either side. The distinct follower/leader profiles arise as leaders only interact through attraction, while followers receive additional alignment information. We further plot the *fluxes*, i.e. the quantities $u^+(x,t) - u^-(x,t)$ and $v^+(x,t) - v^-(x,t)$. In the stationary swarm profile, ($\pm$) movement is balanced such that the swarm maintains its position and shape, see Fig. 7.

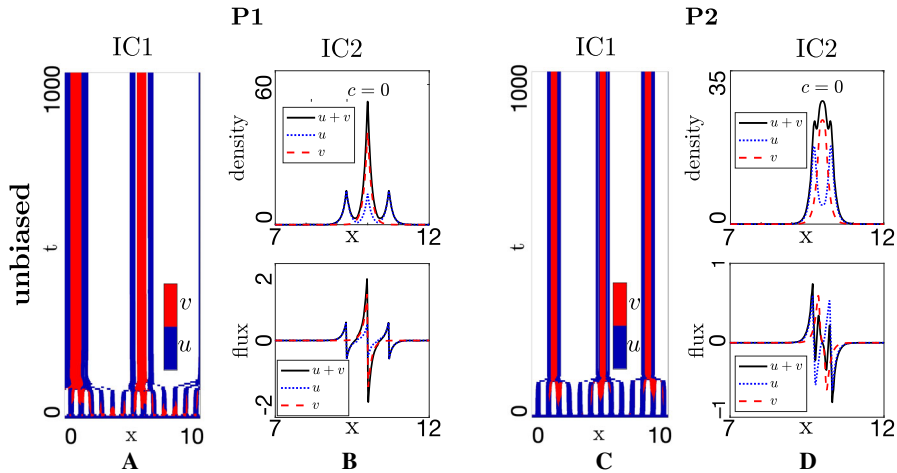[1] These are leaders in name only, as in the unbiased scenario there is no directional bias in force.

Fig. 7 Dynamics of the full-model, unbiased case, obtained for $\varepsilon = 0$, $\beta_- = \beta_+ = 0.1$, $\alpha_- = \alpha_+ = 1$. **a**, **c** Space–time evolution of densities under (IC1) for **a** P1, strong attraction–strong alignment, **c** P2, strong attraction–weak alignment. We note that red or blue regions indicate where the total population $> 2(A_u + A_v)$, i.e. clustering has occurred, with red and blue used to indicate local predominance of leaders and followers, respectively. On the other hand, any regions of white space indicate where the total population is not considered as clustered, i.e. $\leq 2(A_u + A_v)$. Panels **b**, **d** show (top) population distribution and (bottom) population fluxes for solutions under (IC2) for **b** P1, strong attraction–strong alignment, **d** P2, strong attraction–weak alignment. (P1) $q_r = 0$, $q_l = 10$, $q_a = 8$, (P2) $q_r = 0$, $q_l = 1$, $q_a = 10$, with other parameter values set as $A_u = A_v = 1$ (IC1), $M_u = M_v = 12.61$ (IC2), $\lambda_1 = 0.2$, $\lambda_2 = 0.9$ (Color figure online)
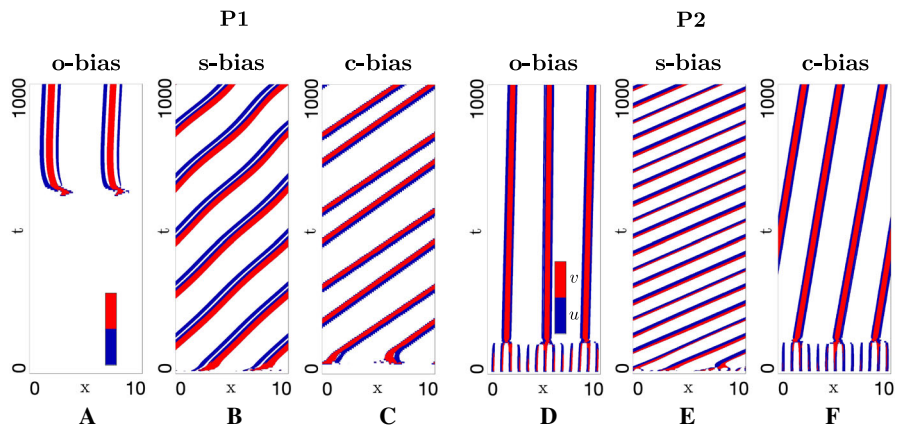

Fig. 8 Impact of biases on swarm movement for the full model in a strong attraction-strong alignment regime (P1), strong attraction–weak alignment regime (P2) and under (IC1). Populations plotted in space–time (colourmap as described in Fig. 7). **a**, **d** O-bias, obtained for $\varepsilon = 0.2$ (s-bias and c-bias inactive, $\beta_- = \beta_+ = 0.1$, $\alpha_- = \alpha_+ = 1$); **b**, **e** s-bias, obtained for $\beta_+/\beta_- = 0.5/0.1$ (o-bias and c-bias inactive, $\varepsilon = 0$, $\alpha_- = \alpha_+ = 1$); **c**, **f** c-bias, obtained for $\alpha_+/\alpha_- = 1.0/0.2$ (o-bias and s-bias inactive, $\varepsilon = 0$, $\beta_- = \beta_+ = 0.1$). Remaining parameters set at (P1) $q_r = 0$, $q_l = 10$, $q_a = 8$, (P2) $q_r = 0$, $q_l = 1$, $q_a = 10$ and $A_u = A_v = 1$, $\lambda_1 = 0.2$, $\lambda_2 = 0.9$

4.2.2 Introduction of Leader Biases

We perform the same set of simulations, but extended to include one of the three proposed mechanisms for leader bias. Simulation results under (IC1) indicate that self-organisation can be maintained under the inclusion of leader-bias, where again we observe that an initially dispersed population aggregates into one or more swarm, see Fig. 8. Notably, these swarms can subsequently migrate through space, indicating that a leader-generated bias can lead to sustained swarm movement. Yet the degree and direction of movement significantly varies with the type (and strength) of bias, demanding a more extensive analysis of when and which type of bias leads to steered swarm movement.

To investigate this in a controlled manner, we force populations into forming an isolated swarm by applying (IC2), ensuring that any subsequent swarm dynamics are the result of internal interactions rather than the influence of neighbouring swarm profiles. Each of the bias strengths are then progressively altered, individually or in concert, under each of our two principal parameter regimes (strong attraction–strong alignment and strong attraction–weak alignment): Figs. 9 and 10, respectively, plot the key behaviours observed for these two regimes.

The dynamics generated by **o-bias** are illustrated in Figs. 9a and 10a. Over a wide range of bias strengths, **o-bias** generates steered swarming, with an increased speed in the target direction as ε increases. However, two caveats must be highlighted. First, under certain parameter combinations we unexpectedly observe swarms that move away from the target, specifically for weaker biases in the weak alignment regime (see Fig. 10a1). Second, excessive biases can lead to loss of swarm coherence and eventual dispersion (see Fig. 9a4). Thus, we conclude **o-bias** is found to be only partially successful in generating a steered swarm.

We next consider **s-bias**, i.e. increasing the ratio of leader speeds when moving towards or away from the target. Indicative simulations are plotted in Figs. 9b and 10b. Similar to **o-bias**, successful steering only occurs within a range of β_+/β_- values. First, as observed above under **o-bias**, certain parameter regimes are capable of generating counter target directed swarms, for example, see Fig. 9b1 for a moderately faster v^+ population in the high attraction–high alignment regime. Second, while increasing the speed ratio can help generate steered swarms, excessively fast target-directed movements can lead to "swarm-splitting", i.e. leaders that pull free from followers and leave them stranded. This phenomenon is observed in Fig. 9b4 at around $T \approx 290$, or in Fig. 10b3 around $T \approx 80$. Under periodic boundary conditions, runaway leaders eventually reconnect with the stranded followers, leading to a periodic cycle (see the illustrative example of Fig. 10b3). Of course, in a real-world scenario, leaders would simply leave followers behind.

Representative swarm behaviours under modulation of **c-bias**, i.e. where we modulate the relative conspicuousness of leaders moving towards or away from the destination, are shown in Figs. 9c and 10c. Notably, this form of bias was found to consistently generate a steered swarm in the target direction, over all tested ranges of α_+/α_- and for both two parameter regimes.

As a final exploration, we examined swarm movement with all biases applied simultaneously: typical results are shown in Fig. 9d for the high attraction-high alignment
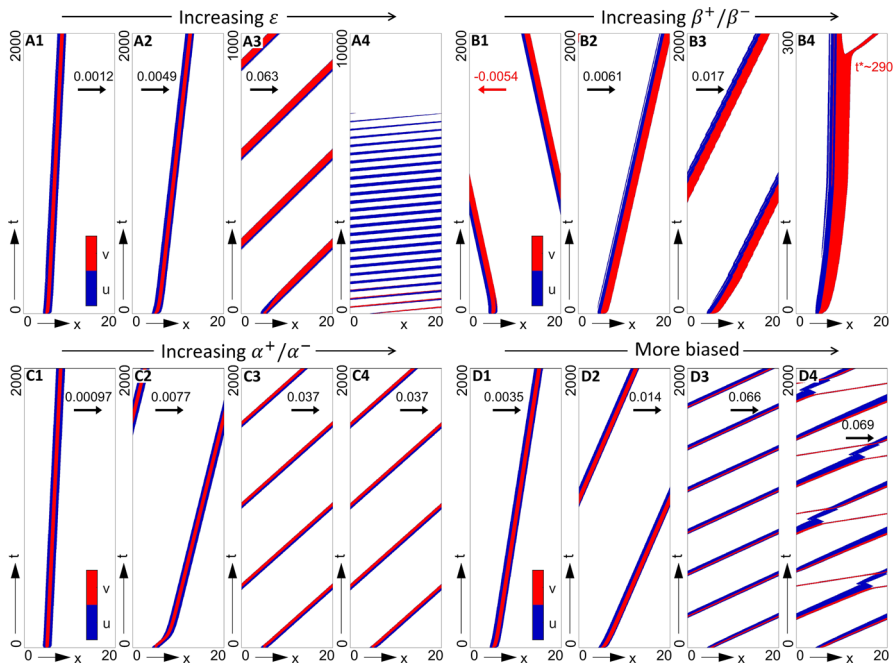
Fig. 9 Impact of biases on swarm movement for the full model in a strong alignment-strong attraction regime (P1) and under (IC2). Populations plotted in space–time (colourmap as described in Fig. 7). Note that we append each plot with the swarm speed, for cases where a travelling wave solution is (numerically) found. **a** O-bias, obtained for $\varepsilon =$ **a1** 0.5, **a2** 1.0, **a3** 2.0, **a4** 3.0 (s-bias and c-bias inactive, $\beta_+ = \beta_- = 0.1, \alpha_+ = \alpha_- = 1$). **b** S-bias, obtained for $\beta_+/\beta_- =$ **b1** 0.2/0.1, **b2** 0.3/0.1, **b3** 0.5/0.1, **b4** 0.6/0.1 (o-bias and c-bias inactive, $\varepsilon = 0, \alpha_+ = \alpha_- = 1$). **c** C-bias, obtained for $\alpha_+/\alpha_- =$ **c1** 1/0.9, **c2** 1/0.575, **c3** 1/0.55, **c4** 1/0 (o-bias and s-bias inactive, $\varepsilon = 0, \beta_+ = \beta_- = 0.1$). **d** Simultaneous biases, for **d1** $\varepsilon = 0.25, \beta_+/\beta_- = 0.15/0.1, \alpha_+/\alpha_- = 1/2/3$, **d2** $\varepsilon = 0.5, \beta_+/\beta_- = 0.2/0.1, \alpha_+/\alpha_- = 1/0.5$, **d3** $\varepsilon = 0.75, \beta_+/\beta_- = 0.25/0.1, \alpha_+/\alpha_- = 1/0.4$, **d4** $\varepsilon = 1, \beta_+/\beta_- = 0.3/0.1, \alpha_+/\alpha_- = 1/(1/3)$. Other parameters are (P1) $q_r = 0, q_l = 10, q_a = 8, M_u = M_v = 12.61, \lambda_1 = 0.2, \lambda_2 = 0.9$

regime only. The application of multiple biases appears to reinforce steered movement in the direction of the destination, for example, overturning the counter-directed swarms obtained for lower ε and ratios of β_+/β_-. Yet escaping leaders can still occur when β_+/β_- becomes too large, e.g. see Fig. 9d4.

5 Discussion

Collective migration occurs when a population formed from interacting individuals self-organise and move in coordinated fashion. Recently, much attention has focused on the presence of leaders and followers, essentially a division of the group into distinct fractions that are either informed and aim to steer or naive and require steering, (Franks et al. 2002; Reebs 2000; Mueller et al. 2013). Here we have formulated a continuous model to understand such phenomena, a non-local hyperbolic PDE system that explicitly incorporates separate leader and follower populations that have dis-
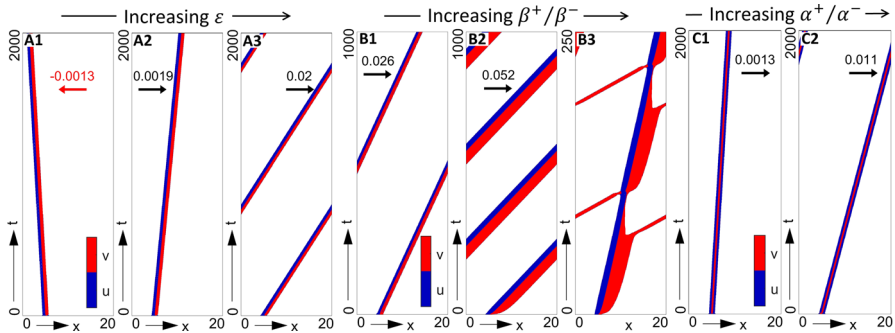
Fig. 10 Impact of biases on swarm movement for the full model in a strong attraction–weak alignment regime (P2) and under (IC2). Populations plotted in space–time (colourmap as described in Fig. 7). Note that we append each plot with the swarm speed, for cases where a travelling wave solution is (numerically) found. **a O-bias**, obtained for $\varepsilon =$ **a1** 3.0, **a2** 5.0, **a3** 15.0 (s-bias and c-bias inactive, $\beta_+ = \beta_- = 0.1, \alpha_+ = \alpha_- = 1$). **b S-bias**, obtained for $\beta_+/\beta_- =$ **b1** 0.2/0.1, **b2** 0.8/0.1, **b3** 1/0.1 (o-bias and c-bias inactive, $\varepsilon = 0, \alpha_+ = \alpha_- = 1$). **c C-bias**, obtained for $\alpha_+/\alpha_- =$ **c1** 1/0.9, **c2** 1/0 (o-bias and s-bias inactive, $\varepsilon = 0, \beta_+ = \beta_- = 0.1$). Other parameters are (P2) $q_r = 0, q_l = 10, q_a = 8, M_u = M_v = 12.61, \lambda_1 = 0.2, \lambda_2 = 0.9$

tinct responses to other swarm members. We considered distinct mechanisms through which leaders attempt to influence the swarm. Specifically, taking inspiration from the guidance provided by scout bees (Seeley 2010; Lindauer 1957), we focused on three different mechanisms: a bias in the leader alignment according to the target (**o-bias**), higher speed (**s-bias**) when moving towards the target and greater conspicuousness (**c-bias**) when moving towards the target.

We initially focused on simpler models of greater analytical tractability. First, a leaders-only model composed only of informed members. Here only o-bias or s-bias operate, both proving effective at steering the group towards the destination. Maintaining group cohesion is, unsurprisingly, contingent on sufficiently strong attraction. Second, we considered a followers-with-implicit-leaders model: population members were naive but received some alignment bias, e.g. due to an implicitly present leader population. The range of dynamics generated by this model is more complicated, stemming from the more sophisticated alignment response. Nevertheless, introduction of bias acts to break the symmetry, significantly favouring the target direction.

The full follower–leader model is capable of forming and maintaining a swarm that is consistently steered towards the destination, across a broad range of parameter regimes. Nevertheless, when examined individually, the distinct biases reveal varying levels of success at generating a steered swarm. First, o-bias and s-bias can, somewhat surprisingly, generate a swarm that moves away from the target, even inside plausible parameter regimes where both attractive and alignment interactions are operating within the swarm. Second, introduction of biases can lead to eventual dispersal of the swarm, pushing the system outside the regime in which attraction maintains swarm cohesion. Third, significant variation in speeds can lead to swarm splitting, where leaders split away from the group and leave followers stranded. Distinctly conspicuous leaders, however, consistently generated swarms moving towards the target, although

we acknowledge the generality of this statement is limited by the purely numerical nature of the study.

The varying success of different influence strategies may stem from the manner in which the biases act. O-bias and s-bias only *indirectly* influence followers: they describe behaviours in which the leaders alter their response according to the target direction, but do not directly enter the dynamics of the follower population. Any influence they exert on followers is therefore through altering the distribution of the leader population with respect to the followers, e.g. a variation in velocity that tends to polarise the position of leaders.

Furthermore, the guidance efficiency provided by o-bias and s-bias appears to be related to the interactions parameter regime. On the one hand, we observed counter-target directed swarms under o-bias in the strong attraction–weak alignment regime. From a mathematical perspective this is reasonable, as the alignment strength (q_l) directly multiplies the orientation bias (ε), see Eqs. 9 and 14 . We therefore speculate that o-bias demands a sufficiently strong alignment. Otherwise, attraction dominates and the swarming group is directed accordingly, potentially against the target, as in Fig. 10a1. On the other hand, s-bias can lead to swarming against the target under strong alignment-strong attraction. In support of this, we remark that swarming direction derives from the transport terms (depending on $\beta_+ : \beta_-$) and the competing social interactions. In summary, we speculate that o-bias is favoured by interactions (specifically, alignment) while s-bias is hindered by them. C-bias, however, *directly* influences the followers: weighting the follower alignment to favour the target direction. For swarming populations, it is worth stressing that these various biases may well act in concert: for example, in the context of bee swarms, speed variation may not be the intended mechanism for generating movement towards the target; it may rather be a side effect of altering the conspicuousness of nest-oriented scouts.

As noted above, biases act to alter the relative positions of leader and follower populations, subtly weighting the interactions to break the symmetry of the system. Different parameter regimes lead to different follower/leader distributions, which we broadly classify as pull and/or push systems: in the former, leaders adopt a position at the front of the swarm, pulling the followers towards the target; in the latter, leaders are primarily concentrated in the rear, pushing them towards the destination. In a third swarm configuration, leaders concentrate in the middle of the swarm: they may be pulling and pushing at the same time. Transitions in the follower–leader distribution are highly contingent on parameter choice: for example, in Fig. 9c2–c3 we observed a sharp transition in the follower–leader distribution under a marginal variation in conspicuousness, in turn generating a significantly faster swarm. A more detailed analytical investigation into these transitions would be of significant interest, but lies outside the scope of the present study.

The model here provides substantial insight into the mechanisms through which informed leaders direct a swarm, yet its complexity has demanded certain simplifications. For example, in this preliminary work we have restricted to fixed leader and follower populations—a reasonable approximation for, say, bee swarms, where a fixed subset of the population has explicit knowledge of the destination. In other instances, follower–leader distinction may be less clearcut and potentially transferable: for example, within cell populations "leadership" may be a chemically acquired

characteristic determined by signals transmitted by other cells or the environment (Atsuta and Takahashi 2015). Extensions of the model in this direction would require additional terms that account for the transfer between follower and leader status. We also note that the model here has focused on a simplified one-dimensional framework, though real-life collective migration phenomena are typically two or three dimensional in structure (for example, in bee swarms the streaker leaders adopt a position concentrated towards the upper portion of a 3D swarm). Further potential adaptations could include incorporating environmental heterogeneity, such as the need to overcome environmental obstacles, or modelling other forms of interaction, such as "chase-and-run" phenomena in which one population attempts to escape a population of pursuers. The latter is certainly relevant in ecological instances, for instance predator–prey relationships, but extends to various cellular populations including neural crest and placode cells (Theveneau et al. 2013). In this respect, a similar approach has been proposed in Eftimie and Coulier (2015) to model inter-individual avoidance and learning tolerance behaviours exhibited by biological groups. However, while discrete models have been formulated to describe chase-and-run processes, e.g. Colombi et al. (2020), a complementary continuous approach may yield further insights. Finally, the model lends itself to studying decision-making, i.e. where swarming may lead to consensus where there are multiple informed leader populations each exhibiting their own preferred direction. A fundamental contribution in this direction has been provided in Couzin et al. (2005) through a discrete description. Notwithstanding its simplifications, we believe the model presented here provides a starting point for future investigations into the role of heterogeneity on collective migration phenomena.

Declaration

Conflict of interest The authors declare that they have no conflict of interest.

A Extended Notation of the Full Model

For ease of reading, we extend the $(\pm)$ notation for the follower–leader model description.

$$
\begin{aligned}
\frac{\partial u^+}{\partial t} + \gamma \frac{\partial u^+}{\partial x} = & -\left(\lambda_0 + 0.5\lambda_2 \tanh\left(y^{u^+} - y_0\right)\right) u^+ \\
& + \left(\lambda_0 + 0.5\lambda_2 \tanh\left(y^{u^-} - y_0\right)\right) u^-,
\end{aligned}
$$

$$\frac{\partial u^-}{\partial t} - \gamma \frac{\partial u^-}{\partial x} = + \left(\lambda_0 + 0.5\lambda_2 \tanh\left(y^{u^+} - y_0\right)\right) u^+$$
$$- \left(\lambda_0 + 0.5\lambda_2 \tanh\left(y^{u^-} - y_0\right)\right) u^-,$$

$$\frac{\partial v^+}{\partial t} + \beta_+ \frac{\partial v^+}{\partial x} = - \left(\lambda_0 + 0.5\lambda_2 \tanh\left(y^{v^+} - y_0\right)\right) v^+$$
$$+ \left(\lambda_0 + 0.5\lambda_2 \tanh\left(y^{v^-} - y_0\right)\right) v^-,$$

$$\frac{\partial v^-}{\partial t} - \beta_- \frac{\partial v^-}{\partial x} = + \left(\lambda_0 + 0.5\lambda_2 \tanh\left(y^{v^+} - y_0\right)\right) v^+$$
$$- \left(\lambda_0 + 0.5\lambda_2 \tanh\left(y^{v^-} - y_0\right)\right) v^-.$$

Initial conditions:

$$u^+(x,0) = u_0^+(x), \quad u^-(x,0) = u_0^-(x), \quad v^+(x,0) = v_0^+(x), \quad v^-(x,0) = v_0^-(x).$$

Turning rates $\lambda_0 = \lambda_1 + 0.5\lambda_2$, with $y^{i^\pm}$, $i \in u, v$ given by

$$y^{u^+} = q_r \int_0^\infty K_r(s)\left(u(x+s) + v(x+s) - u(x-s) - v(x-s)\right)ds,$$
$$- q_a \int_0^\infty K_a(s)\left(u(x+s) + v(x+s) - u(x-s) - v(x-s)\right)ds,$$
$$+ q_l \int_0^\infty K_l(s)\left(u^-(x+s) + \alpha_- v^-(x+s) - u^+(x-s) - \alpha_+ v^+(x-s)\right)ds,$$

$$y^{u^-} = q_r \int_0^\infty K_r(s)\left(u(x-s) + v(x-s) - u(x+s) - v(x+s)\right)ds$$
$$- q_a \int_0^\infty K_a(s)\left(u(x-s) + v(x-s) - u(x+s) - v(x+s)\right)ds,$$
$$+ q_l \int_0^\infty K_l(s)\left(u^+(x-s) + \alpha_+ v^+(x-s) - u^-(x+s) - \alpha_- v^-(x+s)\right)ds,$$

$$y^{v^+} = q_r \int_0^\infty K_r(s)\left(u(x+s) + v(x+s) - u(x-s) - v(x-s)\right)ds,$$
$$- q_a \int_0^\infty K_a(s)\left(u(x+s) + v(x+s) - u(x-s) - v(x-s)\right)ds,$$
$$- 2q_l \int_0^\infty K_l(s)\varepsilon \, ds,$$

$$y^{v^-} = q_r \int_0^\infty K_r(s)\left(u(x-s) + v(x-s) - u(x+s) - v(x+s)\right)ds,$$
$$- q_a \int_0^\infty K_a(s)\left(u(x-s) + v(x-s) - u(x+s) - v(x+s)\right)ds,$$
$$+ 2q_l \int_0^\infty K_l(s)\varepsilon \, ds.$$

Table 3 Table of parameters with fixed values

Parameter	Description	Value [Unit]
y_0	Shift of the turning function	2
s_r	Repulsion range	0.25 [L]
s_l	Alignment range	0.5 [L]
s_a	Attraction range	1 [L]
m_r	Width of repulsion kernel	0.25/8 [L]
m_l	Width of alignment kernel	0.5/8 [L]
m_a	Width of attraction kernel	1/8 [L]
L	Domain length	10 [L]
γ	Follower speed	0.1 [L/T]

The interaction kernels $K_i(s)$, for $i \in r, a, l$, are specified in Eq. (8).

B Fixed Parameters

The parameters in Table 3 are common to all models and set at a fixed reference value, in accordance with those in Eftimie et al. (2007).

C Numerical Method

Numerical simulations are performed on a 1D spatial domain $[0, L]$ with periodic boundary conditions imposed at $x = 0, L$:

$$u^+(0, t) = u^+(L, t), \quad u^-(0, t) = u^-(L, t), \tag{45}$$

and similarly for $v^{\pm}$. The numerical scheme invokes a Methods of Lines approach, where initial discretisation over space yields a system of ordinary differential equations that are subsequently integrated over time. Spatial movement terms are approximated with a first order upwind scheme. Switching terms demand approximation of the infinite attraction/repulsion/alignment integrals. For this we exploit the Gaussian nature of the Kernel functions and approximate the integrals on finite domains $[0, 6i]$, $i = s_r, s_a$, for attractive and repulsive kernels and $[0, 2s_l]$ for alignment. The integral itself is approximated using Simpson's method. We finally remark that under the periodic boundary conditions the integrals are wrapped around the domain.

D Stability Analysis for Followers-with-Implicit-Leaders Model

D.1 Expressions for Stability Analysis

Basic algebra provides the following expressions for $\lambda_{i\pm}^{i\pm}$, for $i \in \{u, v\}$:

$$
\begin{aligned}
\lambda_{u-}^{u+} &= 0.5\lambda_2 \left[1 - \tanh^2(q_l(u^{**} - u^*) - y_0)\right] \left(q_r \hat{K}_r^+(k) - q_a \hat{K}_a^+(k) + q_l \hat{K}_l^+(k)\right), \\
\lambda_{u-}^{u-} &= 0.5\lambda_2 \left[1 - \tanh^2(-q_l(u^{**} - u^*) - y_0)\right] \left(q_r \hat{K}_r^-(k) - q_a \hat{K}_a^-(k) - q_l \hat{K}_l^+(k)\right), \\
\lambda_{u+}^{u+} &= 0.5\lambda_2 \left[1 - \tanh^2(q_l(u^{**} - u^*) - y_0)\right] \left(q_r \hat{K}_r^+(k) - q_a \hat{K}_a^+(k) - q_l \hat{K}_l^-(k)\right), \\
\lambda_{u+}^{u-} &= 0.5\lambda_2 \left[1 - \tanh^2(-q_l(u^{**} - u^*) - y_0)\right] \left(q_r \hat{K}_r^-(k) - q_a \hat{K}_a^-(k) + q_l \hat{K}_l^-(k)\right),
\end{aligned}
\tag{46}
$$

where $\hat{K}_j^{\pm}(k)$, $j = r, a, l$ denote the Fourier transform of the kernel $K_j(s)$, i.e.

$$
\hat{K}_j^{\pm}(k) = \int_{-\infty}^{+\infty} K_j(s)e^{\pm iks}ds = \exp\left(\pm is_j k - \frac{k^2 m_l^2}{2}\right), \quad j = r, a, l. \tag{47}
$$

Substituting Eq. 46 into Eqs. 34 and 35 yields

$$
\begin{aligned}
C(k) = {}&-2\lambda_1 - \lambda_2 - 0.5\lambda_2 \left[\tanh(q_l(u^{**} - u^* - \eta) - y_0)\right. \\
&\left.+ \tanh(-q_l(u^{**} - u^* - \eta) - y_0)\right] \\
&+ q_l(\hat{K}_l^+(k) + \hat{K}_l^-(k)) \left\{u^* \left[0.5\lambda_2(1 - \tanh^2(q_l(u^{**} - u^* - \eta) - y_0))\right]\right. \\
&\left.+ u^{**} \left[0.5\lambda_2(1 - \tanh^2(-q_l(u^{**} - u^* - \eta) - y_0))\right]\right\}
\end{aligned}
\tag{48}
$$

$$
\begin{aligned}
D(k) = {}&4\gamma^2 k^2 + 2\gamma\lambda_2 ik \left\{\tanh(-q_l(u^{**} - u^* - \eta) - y_0)\right. \\
&- \tanh(q_l(u^{**} - u^* - \eta) - y_0) \\
&+ u^*[1 - \tanh^2(q_l(u^{**} - u^* - \eta) - y_0)](-2q_r \hat{K}_r^+(k) + 2q_a \hat{K}_a^+(k) \\
&- q_l \hat{K}_l^+(k) + q_l \hat{K}_l^-(k)) \\
&+ u^{**}[1 - \tanh^2(-q_l(u^{**} - u^* - \eta) - y_0)](2q_r \hat{K}_r^-(k) - 2q_a \hat{K}_a^-(k) \\
&\left.- q_l \hat{K}_l^+(k) + q_l \hat{K}_l^-(k))\right\}.
\end{aligned}
\tag{49}
$$

D.2 Steady-State Variation in Parameter Space

When alignment impacts on the social interactions, i.e. $q_l \neq 0$, Eq. 29 can have one, three or five solutions, depending on the value of λ and η. Specifically, for smaller η two-parameter numerical bifurcation diagrams in (q_l, λ) space indicate a threshold value $\lambda^* \in (0, 1)$ such that if $\lambda > \lambda^*$ then there are up to three solutions. Conversely, if $\lambda < \lambda^*$ there are up to five solutions (Fig. 11a, b). As η increases, the parameter
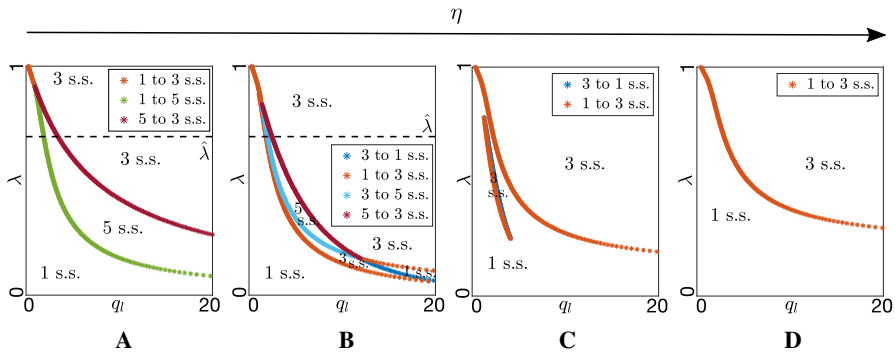
Fig. 11 Two parameter bifurcation diagram in (q_l, λ) space, obtained for **a** $\eta = 0$, **b** $\eta = 0.04$, **c** $\eta = 0.2$, **d** $\eta = 0.4$. Dashed lines in **a**, **b** indicate the value of λ, denoted as $\hat{\lambda}$, resulting from $\lambda_1 = 0.2$ and $\lambda_2 = 0.9$ (compare to bifurcation plots in Fig. 4a and b). The mean total follower density is set as $A_u = 2$
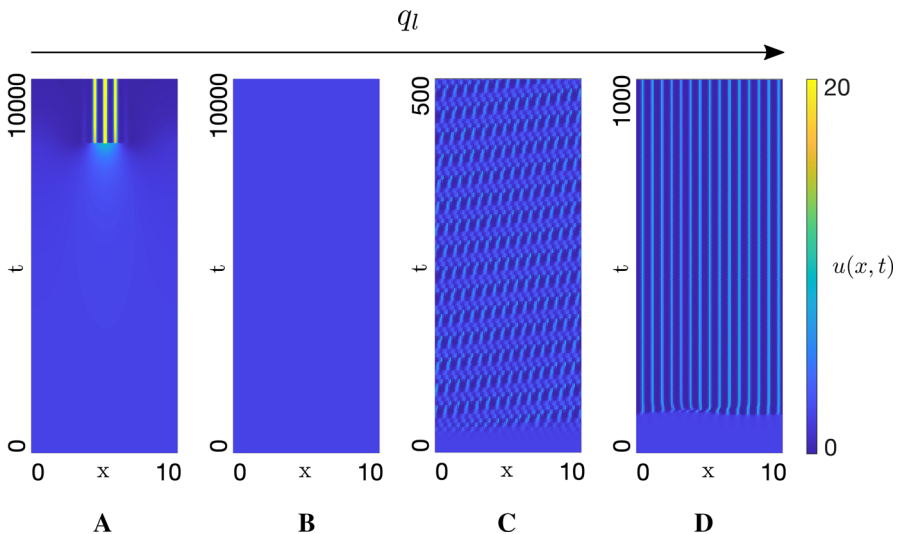

Fig. 12 Pattern formation for the followers-with-implicit-leaders model under the unbiased scenario, i.e. $\eta = 0$, obtained for **a** $q_l = 0.4$, **b** $q_l = 1.3$, **c** $q_l = 2$, **d** $q_l = 2.5$. The other parameters are set as $q_r = 0$, $q_a = 0.25$, $A_u = 2$, $y_0 = 2$, $\lambda_1 = 0.8$, $\lambda_2 = 3.6$. ICs are perturbations of $(u^*, u^{**}) = (1, 1)$ in case (A), (B) and (D). In case (C), ICs are perturbations of $(u^*, u^{**}) = (1.62, 0.38)$

region resulting in 5 steady states reduces, completely disappearing for $\eta = 0.2$, see Fig. 11a, b, c. For $\eta = 0.4$, Eq. 29 shows one or three solutions, see Fig. 11d.

D.3 Effect of Alignment on Equilibrium Points

The bifurcation diagram in Fig. 4a shows that in the absence of any external bias, various stationary and temporal patterns can emerge, as previously described (Eftimie et al. 2007). For example, under weak alignment and sufficiently strong attraction, pattern formation occurs whereby the population aggregates through mutual

attraction (Fig. 12a). Under weak alignment, however, a symmetry is maintained between the proportions of ($\pm$) populations and the aggregate remains stationary. For stronger alignment the HSS becomes stable and the population remains uniformly dispersed across the domain, see Fig. 12b, yet for even stronger alignment two symmetric branches appear with both locally undergoing a saddle point bifurcation and leading to the formation of moving patterns (Fig. 12c). Note, though, for parameters in this region and quasi-symmetrically distributed initial populations, patterns are equally likely to favour the ($+$) or ($-$) directions. Within this alignment range, the central equilibrium turns back to generate stationary aggregations (Fig. 12d) and when the system crosses a critical value a pitchfork bifurcation arises: the solution $(u^*, u^{**}) = (1, 1)$ loses its stability in the homogeneous space and the population jumps to one of the stable branches.

References

Armstrong NJ, Painter KJ, Sherratt JA (2006) A continuum approach to modelling cell–cell adhesion. J Theor Biol 243(1):98–113

Atsuta Y, Takahashi Y (2015) FGF8 coordinates tissue elongation and cell epithelialization during early kidney tubulogenesis. Development 142(13):2329–2337

Beekman M, Fathke RL, Seeley TD (2006) How does an informed minority of scouts guide a honeybee swarm as it flies to its new home? Anim Behav 71(1):161–171

Bernardi S, Colombi A, Scianna M (2018) A particle model analysing the behavioural rules underlying the collective flight of a bee swarm towards the new nest. J Biol Dyn 12(1):632–662

Brent LJN, Franks DW, Foster EA, Balcomb KC, Cant MA, Croft DP (2015) Ecological knowledge, leadership, and the evolution of menopause in killer whales. Curr Biol 25(6):746–750

Carrillo JA, Fornasier M, Toscani G, Vecil F (2010) Particle, kinetic, and hydrodynamic models of swarming. In: Mathematical modeling of collective behavior in socio-economic and life sciences. Springer, pp 297–336

Chen L, Painter KJ, Surulescu C, Zhigun A (2020) Mathematical models for cell migration: a non-local perspective. Philos Trans R Soc B 375(1807):20190379

Cheung KJ, Gabrielson E, Werb Z, Ewald AJ (2013) Collective invasion in breast cancer requires a conserved basal epithelial program. Cell 155(7):1639–1651

Colombi A, Scianna M, Alaia A (2017) A discrete mathematical model for the dynamics of a crowd of gazing pedestrians with and without an evolving environmental awareness. Comput Appl Math 36(2):1113–1141

Colombi A, Scianna M, Painter KJ, Preziosi L (2020) Modelling chase-and-run migration in heterogeneous populations. J Math Biol 80(1):423–456

Couzin ID, Krause J, Franks NR, Levin SA (2005) Effective leadership and decision-making in animal groups on the move. Nature 433(7025):513–516

Couzin ID, Krause J, James R, Ruxton GD, Franks NR (2002) Collective memory and spatial sorting in animal groups. J Theor Biol 218(1):1–12

Dingle H (2014) Migration: the biology of life on the move. Oxford University Press, Oxford

Diwold K, Schaerf TM, Myerscough MR, Middendorf M, Beekman M (2011) Deciding on the wing: in-flight decision making and search space sampling in the red dwarf honeybee *Apis florea*. Swarm Intell 5(2):121–141

Eftimie R (2012) Hyperbolic and kinetic models for self-organized biological aggregations and movement: a brief review. J Math Biol 65(1):35–75

Eftimie R, Coulier A (2015) The role of avoidance and learning behaviours on the formation and movement of biological aggregations. Math Model Nat Phenom 10(2):27–44

Eftimie R, De Vries G, Lewis MA, Lutscher F (2007) Modeling group formation and activity patterns in self-organizing collectives of individuals. Bull Math Biol 69(5):1537

Fetecau RC, Guo A (2012) A mathematical model for flight guidance in honeybee swarms. Bull Math Biol 74(11):2600–2621

Franks NR, Pratt SC, Mallon EB, Britton NF, Sumpter DJT (2002) Information flow, opinion polling and collective intelligence in house-hunting social insects. Philos Trans R Soc B 357(1427):1567–1583

Friedl P, Gilmour D (2009) Collective cell migration in morphogenesis, regeneration and cancer. Nat Rev Mol Cell Biol 10(7):445–457

Friedl P, Locker J, Sahai E, Segall JE (2012) Classifying collective cancer cell invasion. Nat Cell Biol 14(8):777–783

Greggers U, Schoening C, Degen J, Menzel R (2013) Scouts behave as streakers in honeybee swarms. Naturwissenschaften 100(8):805–809

Helbing D, Molnar P (1995) Social force model for pedestrian dynamics. Phys Rev E 51(5):4282

Ioannou CC, Singh M, Couzin ID (2015) Potential leaders trade off goal-oriented and socially oriented behavior in mobile animal groups. Am Nat 186(2):284–293

Janson S, Middendorf M, Beekman M (2005) Honeybee swarms: how do scouts guide a swarm of uninformed bees? Anim Behav 70(2):349–358

Kretz T, Grünebohm A, Kaufman M, Mazur F, Schreckenberg M (2006) Experimental study of pedestrian counterflow in a corridor. J Stat Mech: Theory Exp 2006(10):P10001

Lindauer M (1957) Communication in swarm-bees searching for a new home. Nature 179(4550):63–66

Mogilner A, Edelstein-Keshet L (1999) A non-local model for a swarm. J Math Biol 38(6):534–570

Mueller T, O'Hara RB, Converse SJ, Urbanek RP, Fagan WF (2013) Social learning of migratory performance. Science 341(6149):999–1002

Reebs SG (2000) Can a minority of informed leaders determine the foraging movements of a fish shoal? Anim Behav 59(2):403–409

Schultz KM, Passino KM, Seeley TD (2008) The mechanism of flight guidance in honeybee swarms: subtle guides or streaker bees? J Exp Biol 211(20):3287–3295

Schumacher LJ, Kulesa PM, McLennan R, Baker RE, Maini PK (2016) Multidisciplinary approaches to understanding collective cell migration in developmental biology. Open Biol 6(6):160056

Seeley TD (2010) Honeybee democracy. Princeton University Press, Princeton

Sumpter DJT (2010) Collective animal behavior. Princeton University Press, Princeton

Theveneau E, Steventon B, Scarpa E, Garcia S, Trepat X, Streit A, Mayor R (2013) Chase-and-run between adjacent cell populations promotes directional collective migration. Nat Cell Biol 15(7):763–772

Topaz CM, Bertozzi AL, Lewis MA (2006) A nonlocal continuum model for biological aggregation. Bull Math Biol 68(7):1601

Turing A (1952) The chemical basis of morphogenesis. Philos Trans R Soc B 237:37–72

Vishwakarma M, Di Russo J, Probst D, Schwarz US, Das T, Spatz JP (2018) Mechanical interactions among followers determine the emergence of leaders in migrating epithelial cell collectives. Nat Commun 9(1):1–12

Westley PAH, Berdahl AM, Torney CJ, Biro D (2018) Collective movement in ecology: from emerging technologies to conservation and management. Philos Trans R Soc B 237:20170004